HHS Public Access

Author manuscript

Nature. Author manuscript; available in PMC 2018 October 11.

Published in final edited form as:

Nature. 2018 April ; 556(7701): 326–331. doi:10.1038/s41586-018-0027-0.

Functional circuit architecture underlying parental behaviour

Johannes Kohl[1], **Benedicte M Babayan**[2], **Nimrod D Rubinstein**[1], **Anita E Autry**[1], **Brenda Marin-Rodriguez**[1], **Vikrant Kapoor**[2], **Kazunari Miyamishi**[3], **Larry S. Zweifel**[4], **Liqun Luo**[3], **Naoshige Uchida**[2], and **Catherine Dulac**[1]

[1]Howard Hughes Medical Institute, Department of Molecular and Cellular Biology, Center for Brain Science, Harvard University, Cambridge, Massachusetts 02138, USA

[2]Department of Molecular and Cellular Biology, Center for Brain Science, Harvard University, Cambridge, Massachusetts 02138, USA

[3]Howard Hughes Medical Institute, Department of Biology, Stanford University, Stanford CA 94305, USA

[4]Department of Pharmacology, University of Washington, Seattle, WA 98105, USA; Department of Psychiatry and Behavioral Sciences, University of Washington, Seattle, WA 98105, USA

Summary

Parenting is essential for the survival and wellbeing of mammalian offspring but we lack a circuit-level understanding of how distinct components of this behaviour are orchestrated. Here we investigate how Galanin-expressing neurons in the medial preoptic area ($MPOA^{Gal}$) coordinate motor, motivational, hormonal and social aspects of parenting. These neurons integrate inputs from a large number of brain areas, whose activation depends on the animal's sex and reproductive state. Subsets of $MPOA^{Gal}$ neurons form discrete pools defined by their projection sites. While the $MPOA^{Gal}$ population is active during all episodes of parental behaviour, individual pools are tuned to characteristic aspects of parenting. Optogenetic manipulation of $MPOA^{Gal}$ projections mirrors this specificity, affecting discrete parenting components. This functional organization, reminiscent of the control of motor sequences by pools of spinal cord neurons, provides a new model for how discrete elements of a social behaviour are generated at the circuit level.

Correspondence and requests for materials should be addressed to C.D. (dulac@fas.harvard.edu).

Author Contributions

J.K. and C.D. conceived and designed the study. J.K performed and analyzed tracing and optogenetics experiments. J.K. and B.M.B. performed and analyzed photometry recordings. A.E.A. helped with *in situ* hybridizations, B.M-R. with CTB tracing, N.D.R. with analyzing cTRIO data, and V.K. with optogenetics. L.S.Z., K.M. and L.L. shared unpublished viral reagents. N.U. provided fibre photometry setup. J.K., B.M.B., N.D.R., A.E.A. and C.D. analyzed and interpreted results. J.K. and C.D. wrote the manuscript with input from all authors.

Author Information

The authors declare no competing financial interests.

Main text

Although essential for survival at a multigenerational time scale, parental care entails sacrifices without immediate benefit for the caregiver, suggesting that this behaviour is driven by evolutionarily shaped, hard-wired neural circuits[1,2]. Parenting, like other naturalistic behaviours, comprises multiple coordinated components, such as specific motor patterns, an enhanced motivation to interact with infants, distinct hormonal states and often the suppression of other social activities such as mating. We aimed to exploit the recent identification of $MPOA^{Gal}$ neurons as a key node in the control of parenting in mice[3] to uncover organizational principles of associated neural circuits. We hypothesized that the function of $MPOA^{Gal}$ neurons in parental behaviour requires integration of external signals, such as pup- and other environmental stimuli, with internal hormonal and metabolic information, as well as the ability to orchestrate motor, motivational, hormonal and social components of parenting.

Identity and activity of $MPOA^{Gal}$ inputs

To determine brain-wide inputs into $MPOA^{Gal}$ neurons, we used rabies virus-mediated retrograde trans-synaptic tracing[4] (Fig. 1a), and found that $MPOA^{Gal}$ neurons receive direct inputs from >20 areas in both sexes (Fig. 1b, c, Extended Data Fig. 1a and Extended Data Table 1). Presynaptic neurons within the MPOA itself provided the highest fractional input (~20%), while hypothalamic inputs accounted for ~60% of presynaptic neurons, suggesting extensive local processing (Fig. 1c). $MPOA^{Gal}$ neurons also receive inputs from monoaminergic and neuropeptidergic modulatory areas, the mesolimbic reward system, pathways associated with pheromone-processing, and hypothalamic as well as septal areas involved in emotional states (Fig. 1c and Extended Data Fig. 1a). Inputs from the paraventricular hypothalamic nucleus (PVN), a key area for homeostatic and neuroendocrine control, were particularly abundant. Surprisingly, $MPOA^{Gal}$ neurons did not receive direct inputs from oxytocin (OXT)-secreting PVN neurons (PVN^{OXT}) implicated in parturition, lactation and maternal behaviour[1,2,5], but rather from vasopressin-expressing PVN neurons (PVN^{AVP}), associated with the modulation of many social behaviours[6] and nest building[7] (Fig. 1d). $MPOA^{Gal}$ neurons also received inputs from AVP^{+}, but not OXT^{+}, neurons of the supraoptic nucleus (SON, Extended Data Fig. 1d). Input fractions were similar in males and females, with few exceptions (Fig. 1e, f and Extended Data Fig. 1a). $MPOA^{Gal}$ neurons therefore appear anatomically poised to integrate external (sensory) as well as internal (modulatory) signals relevant to parenting in both sexes.

Next, we investigated $MPOA^{Gal}$ input activation during parenting according to the animal's sex and reproductive state. In laboratory mice, virgin females and sexually experienced males and females are parental, whereas virgin males typically attack and kill pups[3,8,9]. We combined rabies tracing with immunostainings for the activity marker c-Fos after parenting in primiparous females ('mothers'), virgin females, and fathers (Fig. 1g) and compared the $c\text{-}Fos^{+}$ fraction of input neurons between parental animals and non-pup-exposed controls (Fig. 1h–j). Local MPOA inputs were specifically activated during parenting in all groups (Fig. 1h–j), while activation of other inputs was sex- and state-dependent: in parents, but not virgin females, a subset of reward-associated and modulatory inputs were activated (Fig. 1h–

j). Presynaptic neurons in pheromone processing pathways (medial amygdala, MeA; bed nucleus of the stria terminalis, BNST) were selectively activated in fathers and virgin females, but not in mothers (Fig. 1h–j). Since pup-directed aggression in virgin mice is pheromone-dependent[3,8], the MeA-BNST pathway might remain partially active in sexually experienced males and parental virgin females, while fully silenced only in mothers. Intriguingly, the largest number of inputs was activated in fathers (Fig. 1j), and non-overlapping subsets of inputs were activated in mothers and virgin females (Fig. 1h, i). These results suggest that MPOA^{Gal} neurons perform different computations of inputs according to the animal's sex and reproductive state.

Input-output logic of MPOA^{Gal} circuit

To identify MPOA^{Gal} projections and synaptic targets, we infected MPOA^{Gal} neurons with adeno-associated viruses (AAVs) encoding the fluorophore tdTomato as well as the presynaptic marker Syn-GFP (Fig. 2a and Extended Data Fig. 2a). MPOA^{Gal} neurons project to ~20 areas in males and females (Fig. 2b, c and Extended Data Fig. 2b). Many of these regions were previously shown to be involved in maternal behaviour by pharmacological manipulations and lesions, mainly in rats[10] (Extended Data Table 2). Strikingly, this projection map largely overlaps with the input map defined above (Fig. 1c), revealing extensive reciprocal connectivity in parental circuits.

Among the areas most intensely labelled by Syn-GFP were PVN and anteroventral periventricular nucleus (AVPe) (Fig. 2c), both implicated in the control of parenting[6,11]. Using rabies tracing from molecularly defined PVN cell types (Fig. 2d), we found that MPOA^{Gal} neurons project to PVN^{AVP}, PVN^{OXT} and corticotropin-releasing hormone (CRH)-expressing PVN neurons (PVN^{CRH}) in both sexes (Fig. 2e–g). Furthermore, MPOA^{Gal}→PVN connectivity appears sexually dimorphic, with more MPOA^{Gal} neurons projecting to PVN^{AVP} and PVN^{CRH} neurons in males and more MPOA^{Gal} neurons projecting to PVN^{OXT} neurons in females (Fig. 2e–g). MPOA^{Gal} neurons might therefore exert control over parenting-promoting hormonal release in a sex-specific fashion.

Tyrosine-hydroxylase (TH)-expressing neurons in the AVPe were recently found to influence parenting in females via monosynaptic AVPeTH→PVN^{OXT} connections[11]. Rabies tracing from MPOA^{Gal} or AVPeTH neurons showed that while MPOA^{Gal} neurons do not receive monosynaptic inputs from AVPeTH neurons (Fig. 1e), AVPeTH neurons do receive direct inputs from MPOA^{Gal} neurons in both sexes (Extended Data Fig. 2e, f). Thus, MPOA^{Gal} neurons might also influence OXT secretion via a disynaptic MPOA^{Gal}→AVPeTH→PVN^{OXT} circuit (Extended Data Fig. 2g).

We next investigated the organization of MPOA^{Gal} projections, and their activity during parenting. Pairwise injections of the retrograde tracer cholera toxin subunit B (CTB) into MPOA^{Gal} projection targets revealed few double-labelled MPOA^{Gal} neurons (Extended Data Fig. 3a–c). Moreover, retrogradely labelled cell bodies from individual projections occupied characteristic, mostly non-overlapping zones in the MPOA (Extended Data Fig. 3f, g) and conditional tracing from individual projection areas identified only minor collaterals (Extended Data Fig. 4). These results suggest that MPOA^{Gal} neurons are organized in distinct pools, each projecting to largely non-overlapping target areas. To assess whether

different MPOA^{Gal} pools, as defined by their projection sites, were equally activated during parenting, we used Cre-dependent, retrograde canine adenovirus (CAV) to label MPOA^{Gal} subpopulations projecting to regions previously implicated in parenting (12/22 projections, Extended Data Table 2) and quantified their activation in parental females (Fig. 2h). Fractions of c-Fos^{+} neurons differed widely between projections, ranging from >50% (PAG-projecting pool) to <10% (VMH-projecting pool, Fig. 2i). A similar distribution was found in parental fathers (Extended Data Fig. 2d).

Based on their high projection density (Fig. 2c), high activity during parenting (Fig. 2i) and potentially diverse contributions to this behaviour (Extended Data Table 2), we selected MPOA^{Gal} subpopulations projecting to PAG, MeA, VTA and PVN for further characterization. Gal^{+} neurons were ~2× more likely to project to most of these candidate areas than expected from their frequency in the MPOA (Extended Data Fig. 3d, e), supporting the hypothesis that these projections play prominent roles in the control of parenting.

We next aimed to determine whether projection-defined MPOA^{Gal} subpopulations receive selected inputs out of the ~20 identified upstream areas (Fig. 1c) or whether they uniformly integrate all inputs. We used a double-conditional approach in which rabies virus can only infect starter neurons projecting to an area of choice (Fig. 2j and Extended Data Fig. 5b–d)[12]. We found that MPOA^{Gal} projections integrate broad input combinations, with characteristic sets of enriched or depleted inputs (Fig. 2k, l). This is seen for PAG-, MeA-, PVN- and VTA projections, which receive similar, though quantitatively different, inputs (Fig. 2l). Notably, inputs from nucleus accumbens (NAc) and lateral septum (LS), areas involved in reward and emotional responses, respectively, were specifically enriched in VTA-projecting MPOA^{Gal} neurons (Fig. 2k, l). Together, these findings suggest a circuit architecture in which broad input combinations converge onto largely non-overlapping, projection-defined MPOA^{Gal} subpopulations. These subpopulations may in turn be differentially activated during parenting by integrating across quantitatively different sets of activated inputs.

Specific activity of MPOA^{Gal} pools

We next used fibre photometry (Fig. 3a, b)[13,14] to investigate whether individual MPOA^{Gal} subpopulations are active during specific parenting steps. Conditional expression of the calcium reporter GCaMP6m in MPOA^{Gal} neurons was obtained by viral injection (Extended Data Fig. 6a) and an optical fibre implanted above the injection site (Extended Data Fig. 6b–d). The entire ('pan-MPOA^{Gal}') population displayed high activity during all pup-directed parenting episodes in mothers, virgin females and fathers (Fig. 3c–g and Supplementary Video 1), but not during non-pup-directed (nest building) or passive (crouching) parenting episodes (Fig. 3h, i). MPOA^{Gal} activation was stimulus-specific: interactions with adults resulted in minimal activity (Extended Data Fig. 6k, l). Moreover, orofacial motor actions similar to pup interactions did not activate MPOA^{Gal} neurons, confirming that the observed signals were not motion-related. The tuning of MPOA^{Gal} neurons during parenting was similar in all three groups (Fig. 3q) – highlighting their common role in the control of parental interactions. Activation during pup sniffing was higher in mothers than in virgin

females and fathers (Fig. 3c), possibly reflecting the extraordinary sensitivity of postpartum females to pup stimuli (Extended Data Fig. 7)[15]. Further, activity decreased in mothers – but not in fathers – during eating, self-grooming and sniffing of food (Fig. 3j–l). MPOA^{Gal} neurons receive their second-largest fractional input from the arcuate nucleus (Arc), a feeding control centre[16] (Fig. 1c and Extended Data Figure 1a), suggesting that inhibition from circuits controlling mutually exclusive motor patterns, such as eating and pup grooming, might cause this decrease in activity.

To record the activity of projection-defined MPOA^{Gal} subpopulations, we injected MPOA^{Gal} target areas with a Cre-dependent, GCaMP6-expressing herpes simplex virus (HSV) and implanted an optical fibre above the retrogradely labelled cell bodies (Fig. 3m and Extended Data Fig. 6e–h). PAG-projecting MPOA^{Gal} neurons were specifically activated during pup grooming (Fig. 3n and Extended Data Fig. 6m–q), while MeA-projecting MPOA^{Gal} neurons were active during most episodes of parental behaviour (Fig. 3p and Extended Data Fig. 6m–q), indicating a more general role in parenting. Consistent with their weak c-Fos activation after parenting (Fig. 2i), no significant activity changes were detected in VTA-projecting MPOA^{Gal} neurons (Fig. 3o and Extended Data Fig. 6m–p). Nevertheless, MPOA^{Gal}→VTA neurons were weakly responsive during nest entering in a subset of animals (Fig. 3o and Extended Data Fig. 6q; 4/12 mice), potentially reflecting the expectation or drive to interact with pups. Altogether, these findings support the notion that MPOA^{Gal} neurons form functionally distinct modules tuned to specific parenting episodes.

Functionally distinct MPOA^{Gal} pools

We tested this hypothesis by optogenetically activating PAG-, VTA- and MeA projections during pup interactions (Fig. 4a). We virally expressed channelrhodopsin-2 (ChR2) in MPOA^{Gal} neurons (Extended Data Fig. 8a), and implanted optical fibres above MPOA^{Gal} projection targets. Optogenetic activation of PAG projections did not affect the fraction of parental virgin females but suppressed pup attacks in infanticidal virgin males (Fig. 4b), and – consistent with MPOA^{Gal}→PAG activity during parenting (Fig. 3n) – increased pup grooming and pup-directed sniffing bouts in both sexes (Fig. 4c and Extended Data Fig. 8c). Next, we assessed the motivation to interact with pups by inserting a climbable barrier in the home cage between the test animal and pups (Fig. 4d). MPOA^{Gal}→PAG activation had no effect on the number of barrier crosses (Fig. 4d). Importantly, the effects of MPOA^{Gal}→PAG activation were specific to pup interactions, and did not affect interactions with adult conspecifics (Fig. 4e, f).

By contrast, activation of MPOA^{Gal}→VTA projections did not affect pup interactions (Fig. 4g, h), but increased barrier crossing in both sexes (Fig. 4i and Supplementary Video 2), indicating an increase in the motivation to interact with pups. Interestingly, virgin males still exhibited pup-directed aggression after crossing the barrier, suggesting that this effect is not contingent upon the display of parenting. Nevertheless, in naturalistic situations, MPOA^{Gal} neurons and associated VTA projections are activated exclusively during parental interactions, thus specifically mediating parental drive. MPOA^{Gal}→VTA activation did not increase locomotion (Extended Data Fig. 8j, k) and did not affect interactions with intruders of either sex (Fig. 4j, k).

Finally, activation of MPOA^{Gal}→MeA projections neither affected pup-directed behaviours (Fig. 4l, m and Extended Data Figure 7f, g) – except for a decrease in females in time spent in nest (Extended Data Fig. 8f) – nor the motivation to interact with pups (Fig. 4n). However, this manipulation significantly inhibited male-male aggression and chemoinvestigation of a male intruder in females (Fig. 4o, p). Thus, rather than directly influencing parental behaviour, MPOA^{Gal}→MeA activation inhibits social interactions with adult conspecifics.

We tested the necessity of these subpopulations for discrete behaviours by expressing the inhibitory opsin eNpHR3.0 in MPOA^{Gal} neurons and stimulating their projections in virgin females (Fig. 4q, t, w). In accordance with ChR2 data, optogenetic inhibition of MPOA^{Gal}→PAG projections significantly reduced pup grooming and pup-directed sniffing bouts (Fig. 4s and Extended Data Fig. 8n), without affecting other behaviours (Fig. 4r and Extended Data Fig. 8n–p, u). In contrast, inhibition of MPOA^{Gal}→VTA projections specifically reduced barrier crossing frequency (Fig. 4v, u and Extended Data Fig. 8q, r, v), except for a reduction in time spent in nest (Extended Data Fig. 8q). Finally, inhibition of MPOA^{Gal}→MeA projections did not affect interactions with an intruder (Fig. 4y) or other behaviours (Fig. 4× and Extended Data Fig. 8s, t, w). Recent findings indicate that representations of social stimuli in MeA and hypothalamic centres change significantly after sexual experience[17,18]. Thus, low basal activity in this circuit branch in virgin females compared to mothers may preclude further inhibition. Alternatively, or additionally, this lack of effect may result from a more complex role of MPOA^{Gal}→MeA connectivity.

Concluding remarks

Altogether, our data suggest that distinct MPOA^{Gal} pools control discrete aspects of parental behaviour in both sexes (Fig. 5): (1) Consistent with a role of the PAG in motor aspects of maternal behaviour[2], MPOA^{Gal}→PAG projections promote pup grooming. Retrograde tracing from PAG showed that MPOA^{Gal} neurons synapse with GABAergic (inhibitory), but not glutamatergic (excitatory) PAG neurons (Extended Data Fig. 2h–j). Since the vast majority (~90%) of MPOA^{Gal} neurons are GABAergic[3], pup grooming is likely elicited by disinhibition in the PAG. Indeed, PAG infusion of the $GABA_A$ receptor antagonist bicuculline increases pup licking and grooming[19]. (2) In contrast, MPOA^{Gal}→PAG projections specifically influence the motivation to interact with pups without affecting the quality of adult-infant interactions. This is consistent with the postulated role of the VTA in motivation[20] and social reinforcement[21], and complements previous findings in rats[2,22]. Nearby Gal^+ neurons in the lateral hypothalamus promote food-seeking behaviour, despite lacking VTA-projections[23], further highlighting the specific role of MPOA^{Gal} neurons in parenting. (3) Finally, we found that MPOA^{Gal}→MeA projections do not directly influence pup-directed behaviour but rather inhibit potentially competing adult social interactions. Interestingly, MPOA^{Gal}→MeA neurons are active during most episodes of parenting (Fig. 3p, q), suggesting that the entire behaviour, rather than specific parenting components, are broadcast by this projection to influence the vomeronasal pathway[24–26]. Specific inhibitory feedback from MPOA^{Gal} neurons to MeA might impair the detection, or alter the valence, of non-pup-related social stimuli. Indeed, optogenetic stimulation of glutamatergic neurons in the posteriodorsal MeA – the MeA compartment most densely innervated by MPOA^{Gal}

fibres (Fig. 2b) – has been shown to suppress interactions with adult conspecifics[27]. The projections investigated here mediate crucial, non-overlapping aspects of parental behaviour and the sum of their activity profiles matches that of the entire MPOA^{Gal} population (Fig. 3q). Thus, combined with the finding that MPOA^{Gal} neurons contact AVP-, OXT- and CRH-expressing PVN neurons (Fig. 2e–g), we have dissected circuit branches for four major – motor, motivational, social and neuromodulatory – aspects of parenting control. Other MPOA^{Gal} projections not included here may play additional roles in parenting. Lastly, our tracing data suggest extensive connectivity within the MPOA (Fig. 1c), hinting at interactions between functionally specialized MPOA^{Gal} subpopulations.

Considerable progress has recently been made in identifying neuronal populations controlling specific social behaviours or homeostatic functions[10,16,28–31]. However, little is known about how these multi-component behaviours or functions are orchestrated at the circuit level. Intriguingly, the modular architecture uncovered here for the control of parenting is reminiscent of the motor circuit motif identified in the mammalian spinal cord, where discrete phases of locomotor sequences are controlled by functionally distinct neuronal pools with highly specific connectivity patterns[32]. Whether other social behaviours rely on similar circuit architecture remains to be determined.

Methods

Animals

The *Gal::Cre* BAC transgenic line (STOCK Tg(Gal-cre)KI87Gsat/Mmucd, 031060-UCD) was imported from the Mutant Mouse Regional Resource Center and is described in ref. 3. Cre-dependent tdTomato reporter mice (*Gt(ROSA)26Sor*$^{tm9(CAGtdTomato)Hze}$)[33], *C57BL/6J*, *Oxt-ires-Cre, Vgat-ires-Cre* and *TH-ires-Cre* mice were obtained from Jackson Laboratories. *Vglut2-ires-Cre* mice were provided by B. Lowell. The *Avp-ires-Cre* line is described in ref. 7. *Crh-ires-Cre* mice were obtained from B. Lowell, J. Majzoub and Jackson Laboratories. Animals were maintained on 12 h:12 h light/dark cycle (lighted hours: 02:00 – 14:00) with food and water available *ad libitum*. Animal care and experiments were carried out in accordance with the NIH guidelines and approved by the Harvard University Institutional Animal Care and Use Committee (IACUC).

Histology and immunostaining

Animals were perfused transcardially with phosphate buffered saline (PBS) followed by 4% paraformaldehyde (PFA) in PBS. Brains were dissected and post-fixed in 4% PFA for 16 h, then washed in PBS for 6 h. After embedding in 4% low melting point agarose (Thermo Fisher Scientific, 16520-050) in PBS, 60 μm coronal sections were cut on a vibratome (Leica) and mounted on Superfrost Plus slides (VWR, 48311-703) with DAPI-containing Vectashield mounting medium (Vector Laboratories, H-1200). For immunostaining in 48-well culture plates, sections were permeabilized for 30 min in PBS-T (0.3% Triton X-100 in PBS), post-fixed with PFA for 10 min, and washed in PBS-T (3 × 20 min). Blocking was o/n in blocking buffer (0.3 Triton X-100, 1% BSA, 2% normal donkey serum in PBS). Incubation with primary antibodies was performed for 24 – 48 h on a nutator at 4°C. After washing in PBS-T (5 × 60 min), secondary antibodies were added for 48 h at 4°C. After

final washes in PBS-T (5 × 60 min), sections were mounted. Primary antibodies: goat anti-c-Fos (Santa Cruz, sc-52) 1:500, chicken anti-GFP (Abcam, ab13970) 1:1,000, rabbit anti-AVP (Immunostar, 20069) 1:6,000, rabbit anti-OXT (Immunostar, 20068) 1:6,000. Secondary antibodies (all from Thermo Fisher): Alexa-568 anti-goat (A-11057) 1:1,500, Alexa-555 anti-goat (A-21432) 1:1,500, and Alexa-647 anti-goat (A-21447) 1:1,500. All antibodies were incubated in PBS-T, with the exception of c-Fos antibody, which was incubated in PBS.

RNA *in situ* hybridization

Freshly dissected brains were embedded in OCT (Tissue-Tek, 4583) and frozen with dry ice. 16 μm cryosections were collected on Superfrost Plus slides (VWR, 48311-703) and used for mRNA *in situ* hybridization. Fluorescent mRNA *in situ* hybridization was performed largely as described[24]. Complementary DNA (cDNA) of *Gal* or *EYFP* mRNA was cloned in approximately 800-base-pair segments into pCRII-TOPO vector (Thermo Fisher, K465040). Antisense complementary RNA (cRNA) probes were synthesized with T7 (Promega, P2075) or Sp6 polymerases (Promega, P1085) and labelled with digoxigenin (DIG, Roche 11175025910) or fluorescein (FITC, Roche 11685619910). Hybridization was performed with 0.5 – 1.0 ng ml^{-1} cRNA probes at 68°C. Probes were detected using horseradish peroxidase (POD)-conjugated antibodies (anti-FITC-POD, Roche 11426346910, 1:250; anti-DIG-POD, Roche 11207733910, 1:500). Signals were amplified using biotin-conjugated tyramide (Perkin Elmer NEL749A001KT) and subsequently visualized with Alexa Fluor 488-conjugated streptavidin (Thermo Fisher, S11223), or the TSA-plus Cy3 system (Perkin Elmer, NEL744001KT).

Viruses

Recombinant AAV vectors were produced by the UNC Vector Core. AAV titres ranged from 1.3 to 2.6 × 10^{12} viral particles ml^{-1}, based on quantitative PCR analysis. Pseudotyped, G-deleted rabies virus[4] was obtained from the Salk vector core at a titre of 4.3 × 10^{8} viral particles ml^{-1}. The *pAAV-CAG-FLEx-Syn-GFP* plasmid was kindly provided by Silvia Arber (Friedrich Miescher Institute, Basel) and AAV1/CAG-FLEx-Syn-GFP was produced by the UNC Vector Core. The *pAAV-CAG-FLEx-TCB*, *pAAV-CAG-FLEx-RG*[34], *pAAV-CAG-FLEx^{FRT}-TC* and *pAAV-CAG-FLEx^{FRT}-RG* plasmids were provided by Liqun Luo (Stanford University), and AAV5/DJ-hSyn1-FLEx^{FRT}-mGFP[35]; AAV1/CAG-FLEx^{FRT}-TC and AAV1/CAG-FLEx^{FRT}-RG were packaged by the UNC Vector core. Liqun Luo and Eric Kremer (IGMM, Montpellier) provided CAV2-FLEx^{loxP}-Flp. Larry S. Zweifel (University of Washington) provided CAV2-FLEx-ZsGreen. AAV1/CAG-FLEx-tdTomato, AAV1/Syn-FLEx-GCaMP6m, AAV5/EF1α-DIO-hChR2(H134R)-EYFP and AAV5/EF1α-DIO-EYFP were purchased from UPenn Vector core. HSV-hEF1α-LSL1-GCaMP6m (HT) was obtained from MIT Vector Core.

Anterograde tracing

Anterograde tracing experiments were performed in *Gal::Cre* mice (or in *C57BL/6J* for control experiments) at ~8–12 weeks of age. All surgeries were performed under aseptic conditions in animals anesthetized with 100 mg kg^{-1} ketamine (KetaVed, Vedco) and 10 mg kg^{-1} xylazine (AnaSed) via intra-peritoneal (i.p.) injection. Using a Nanoject II injector

(Drummond Scientific), 300 nl of a 1:1 mixture of AAV1/CAG-FLEx-tdTomato and AAV1/CAG-FLEx-Syn-GFP[36] (Synaptophysin-GFP) was injected into the MPOA (coordinates: AP: 0.0, ML: −0.5, DV: −5.05 mm) to visualize presynaptic terminals of $MPOA^{Gal}$ neurons. Syn-GFP was chosen to distinguish presynaptic sites from fibres of passage. Analgesia (buprenorphine, 0.1 mg kg^{-1}, i.p.) was administered for 2 d following each surgery. Two weeks later mice were sacrificed and dissected. In some experiments, a 1:1 mixture of AAV1/CAG-FLEx-tdTomato and AAV1/CAG-FLEx-Syn-GFP was injected to visualize presynaptic terminals of $MPOA^{Gal}$ neurons. For quantification of synaptic density, the average pixel intensity in a target region containing presynaptic GFP^+ punctae was calculated and background-subtracted. Since injections were unilateral and no labelling was observed in most cases contralaterally, the equivalent region on the contralateral hemisphere was chosen for background subtraction; in cases where contralateral GFP^+ punctae were present, an adjacent unlabelled region was chosen. Background-corrected intensities were normalized to the average pixel intensity at the MPOA injection site for each brain.

Trans-synaptic retrograde tracing

Input tracing experiments were performed in *Gal::Cre* mice (or *C57BL/6J* in control experiments) at ~8–12 weeks of age. We injected 150 – 200 nl of a 1:1 mixture of AAV1/CAG-FLEx-TC^B and AAV1/CAG-FLEx-RG unilaterally into the MPOA. Two weeks later, 450 – 600 nl EnvA-pseudotyped, RG-deleted, GFP-expressing rabies virus (EnvA-ΔG-rabies) was injected into the MPOA. After recovery, mice were housed in a biosafety-level-2 (BL2) facility for 4 d before sacrificing. Relative input strength was quantified as follows from brain sections: every second 60 μm section was imaged and cells were counted using the ImageJ CellCounter plugin. GFP^+ cells on the injected hemisphere were counted and assigned to brain areas based on classifications of the Paxinos Mouse Brain Atlas (3rd edition), using anatomical landmarks in the sections visualized by DAPI staining and tissue autofluorescence. In addition, all contralateral and non-assigned GFP^+ cells were counted to obtain the total number of GFP^+ cells. We then quantified the number of ipsilateral $mCherry^+$ starter neurons per brain area and the total number of starter neurons. Since starter neurons are both GFP^+ and $mCherry^+$, while presynaptic neurons are only GFP^+, the total number of starter neurons was subtracted from the total number of GFP^+ neurons to obtain the total number of presynaptic neurons within the MPOA. Finally, the relative input fraction for each area was determined by dividing the number of presynaptic neurons detected in that brain area by the total number of presynaptic neurons in a given brain. Injection of starter AAVs and EnvA-ΔG-rabies into the MPOA of *C57BL/6J* mice did not result in detectable background labelling (Extended Data Fig. 5a). Inputs from PAG were detected only in a subset of animals. Presynaptic AVP^+ neurons in the PVN were identified as predominantly magnocellular based on cell body size[37,38] and -position[39]. Presynaptic neurons in the MPOA (Fig. 2d–g and Extended Data Fig. 2e–j) were identified as Gal^+ by *in situ* hybridization.

Lateralisation effects

Retrograde and anterograde tracing experiments were performed in the right hemisphere. However, a recent study found that OXT receptor is more highly expressed in the left auditory cortex of females and that OXT binding there is crucial for pup retrieval[5]. We

therefore investigated potential lateralisation effects by tracing from MPOA^{Gal} neurons in the left hemisphere. Resulting presynaptic neuron numbers and projection patterns (Extended Data Figs. 1b, 2c) were indistinguishable from those obtained after right-hemispheric tracing, suggesting that anatomical lateralisation is not a dominant feature of the subcortical circuits described here.

Projection-specific trans-synaptic retrograde tracing

For projection-specific trans-synaptic retrograde tracing (cTRIO)[12], 300 – 500 nl of CAV2-FLEx^{loxP}-Flp was injected into identified target areas of MPOA^{Gal} neurons (coordinates, see Extended Data Table 1) in 8 – 12 week old *Gal::Cre* animals. During the same surgery, 300 – 600 nl of a 1:1 mixture of AAV1/CAG-FLEx^{FRT}-TC and AAV1/CAG-FLEx^{FRT}-RG[12] (starter AAVs) was injected into the MPOA. This combination of Cre-dependent, Flp-expressing CAV and Flp-dependent starter AAVs renders MPOA^{Gal} neurons projecting to a specific target area susceptible to subsequent infection with G-deleted, EnvA-pseudotyped rabies virus. Two weeks later, 450 – 500 nl of EnvA-ΔG-rabies was injected into the same MPOA coordinate. After recovery, mice were housed in a biosafety-level-2 (BL2) facility for 4 d before sacrificing. Injection of starter AAVs without CAV did not result in expression (Extended Data Fig. 5b, c). However, since injection of all cTRIO tracing viruses into *C57BL/6J* mice resulted in background expression near the injection site (Extended Data Fig. 5d), the following areas were excluded from analysis: MPOA, BNST, AH, PVN and SON. This background labelling is likely due to low levels of *Cre*- or *Flp*-independent expression of *TVA-mCherry* and *RG*[12].

We quantified the connectivity of each MPOA^{Gal} projection to its inputs using a multinomial regression model (response: neuron counts in each input area, factors: MPOA^{Gal} projections). The baseline category in the model was represented by the mean input fraction across all experiments. Reported effects are therefore relative to a randomly chosen projection and the *P* values reported in Fig. 2k, l are obtained from a normal distribution where the Z-scores are the effects of the multinomial regression divided by their corresponding standard errors. In order to test for differences in the multinomial distribution of input to target region projections, the least-square means from the multinomial regression model was computed using the *lsmeans* package in R and used to run all pairwise comparisons.

MPOA^{Gal} input activity screen

To determine which fraction of MPOA^{Gal} inputs is activated during parental behaviour, viral injections were performed as described in 'Trans-synaptic retrograde tracing'. Animals were single-housed until behavioural testing 4 d later with two pups (see 'Parental behaviour assay'). For the equivalent experiments in mothers and fathers, 8 – 12 week old *Gal::Cre* males and females were paired up 10 d before injection of starter viruses and returned to their home cage where they remained until 3 d after injection of EnvA-ΔG-rabies when either the father and litter (for testing of mothers) or the mother and litter (for testing of fathers) were removed from the home cage. Parents underwent behavioural testing on the following day, i.e. 4 d after injection of EnvA-ΔG-rabies. Typically ~80% of virgin females and >90% of mothers and fathers were parental. 90 min after onset of retrieval, mice were

deeply anesthetized with isoflurane and rapidly perfused transcardially with 30 ml of ice-cold PBS, followed by 30 ml of ice-cold PFA (4% in PBS). Brains were dissected and post-fixed in PFA (4% in PBS) at 4 °C for 16 h. On the next day, brains were rinsed with cold PBS and 60 μm coronal sections were prepared with a vibratome (Leica VT1000 S). Sections were further post-fixed in PFA (4% in PBS) at room temperature for 10 min and immunostainings against c-Fos were performed (see 'Histology and immunostaining'). Only brains from mice that performed all steps of pup-directed parental behaviour (sniffing, retrieval, grooming, licking, crouching) were processed. Animals that were habituated in the test arena but not exposed to pups served as negative controls. Unpaired *t*-tests were used to assess activation of input areas between parental and control animals and *P* values were adjusted for multiple comparisons using the Benjamini-Hochberg method (false-discovery rate, FDR < 0.05).

Previous studies have reported that the basic properties of ΔG-rabies –infected neurons are not altered until 7 d post-infection[40,41] and likewise, effects of rabies on (transgene) expression levels have only been reported 7 d after infection[42]. Since animals were tested and perfused 4 d after rabies infection in our study, neuronal physiology and c-Fos activation should be largely unaffected. Because we reliably observed c-Fos immunostaining in rabies$^+$ neurons (Fig. 1g–j), rabies infection *per se* does not preclude activity-dependent c-Fos expression after 4 d. However, rabies infection could theoretically upregulate c-Fos expression in infected neurons, resulting in an overestimation of activated input neurons in our data set. In order to address this possibility, we compared c-Fos$^+$ cell numbers in the MPOA of unilaterally rabies-injected mothers between the injected (ipsilateral) and the non-injected (contralateral) hemisphere (Extended Data Fig. 1c, upper). We found that numbers of c-Fos$^+$ neurons were not significantly different between hemispheres (Extended Data Fig. 1c, lower; $P = 0.43$; paired *t*-test; n = 6). Therefore, rabies infection is unlikely to strongly affect c-Fos$^+$ expression in our experimental paradigm.

MPOA^{Gal} projection activity screen

In order to determine the activation of individual MPOA^{Gal} projections during parental behaviour, 300 – 500 nl of CAV2-FLEx-ZsGreen was injected into identified MPOA^{Gal} target areas in 8 – 12 week old *Gal::Cre* females. Animals were single-housed one week after injection. Behavioural testing with two pups (see Parental behaviour assay') was performed three weeks after injection to allow for efficient retrograde transport of the virus. For the equivalent experiments in fathers, 8 – 10 week old *Gal::Cre* virgin males were individually paired up with females for 4 d, injected and subsequently returned to the female. 2 – 3 d after pups were born (~3 weeks after injection), and 1 d before testing, the female and pups were removed from the cage. Testing, brain collection and immunostaining was performed as described in 'MPOA^{Gal} input activity screen'. Since MPOA^{Gal} neurons are not activated in non-pup-exposed mice[3], negative controls were not performed in these experiments.

Axon collateralization experiments

In order to assess axon collateralization of MPOA^{Gal} neurons (Extended Data Figure 4), *Gal::Cre* mice received injections of 300 – 500 nl of CAV-FLEx^{loxP}-Flp into an MPOA^{Gal}

target site (coordinates, see Extended Data Table 1), and of 600 nl of AAV5/hSyn1-FLEx^{FRT}-mGFP into the MPOA. Mice were sacrificed 8 weeks later and the signal was amplified by anti-GFP immunostaining.

CTB tracing

Mice expressing *tdTomato* in Gal^{+} neurons (*Gal::Cre$^{+/-}$; loxP-Stop-loxP-tdTomato$^{+/-}$*) received pairwise injections of 50 – 100 nl of 0.5% (wt/vol) fluorescently labelled cholera toxin B subunit (CTB-488, Thermo Fisher C22841, CTB-647, Thermo Fisher C34778). After 7 d, brains were collected, fixed and 60 μm sections prepared. Individual sections were fixed again in 4% PFA for 10 min. The fraction of double-labelled, tdTomato^{+}, Gal^{+} neurons in the MPOA was quantified. In control experiments, a 1:1 mixture of CTB-488 and CTB-647 was injected into MeA or PAG.

Imaging and image analysis

Samples were imaged using an Axio Scan.Z1 slide scanner (Zeiss), and confocal stacks were acquired on an LSM 880 confocal microscope (Zeiss). Image processing was performed using custom routines for the Fiji distribution of ImageJ. For most tracing experiments, every second section was imaged, with the exception of MPOA^{Gal} projection activity and CTB tracing experiments, where every MPOA-containing section was imaged and analyzed.

Parental behaviour assay

Before behavioural testing animals were housed individually for 5 – 7 d unless otherwise specified. Experiments started at the beginning of the dark phase and were performed under dim red light. Testing was performed in the home cage (with the exception of locomotion assays, see below) and preceded by a 30 min habituation period. Two 1 – 4 d old *C57BL/6J* pups were placed in different corners opposite the nest. Once retrieval occurred, a timer was started. Each test was recorded using a multi-camera surveillance system (GeoVision GV-1480) and behaviours were scored by an individual blind to the genotype using the Observer 5.0 or XT 8 software (Noldus Information Technology).

Fibre photometry

Fibre photometry (fluorometry) was performed as previously described[43]. For photometry recordings, 8 – 12 week old *Gal::Cre$^{+/-}$; loxP-Stop-loxP-tdTomato$^{+/-}$* mice were used. For pan-MPOA^{Gal} recordings, 400 – 500 nl of AAV1/Syn-FLEx-GCaMP6m (Upenn Vector Core) was injected into the MPOA; for projection-specific recordings, 600 – 700 nl of hEF1α-LS1L-GCaMP6m, a Cre-dependent, retrograde, long-term Herpes Simplex Virus (LT-HSV) was bilaterally injected into MPOA^{Gal} target areas. During the same surgery, a custom 400 μm fibre-optic cannula (Doric Lenses) was implanted into the MPOA (for coordinates, see Extended Data Table 1). For recordings in mothers and fathers, animals were paired up 5 d before surgery, to ensure that pups were born ~3 weeks after virus injection. One day after surgery, animals were returned to their mating partner. The implanted animal's mating partner and offspring were removed 3 – 5 h prior to recordings. Virgin female mice were single-housed 7 d before the first recording session and thereafter between experiments. Recordings were made 2 – 4 weeks after the surgery under IR

illumination in the mouse's home cage. Mice were briefly (~10 min) habituated in the recording setup before 8 – 10 pups (1 – 4 d old) were introduced into the cage. Recording sessions typically lasted 10 – 20 min, with at least 2 d between sequential recordings. The implant was coupled to a custom patch cord (Doric Lenses) to simultaneously deliver 473 nm excitation light from a DPSS laser (Opto Engine LLC, UT, USA), passed through a neutral density filter (4.0 optical density, Thorlabs, NJ, USA), and to collect fluorescence emission. Activity-dependent fluorescence emitted by cells in the vicinity of the implanted fibre tip was collected by a 0.65 NA microscope objective (Olympus), spectrally separated from the excitation light using a dichroic mirror (Chroma, NY, USA), passed through a band pass filter (ET500/50, Chroma) and focused onto a photodetector (FDS10×10, Thorlabs) connected to a current preamplifier (SR570, Stanford Research Systems). Another band pass filter (ET600/20) in front of a second photodetector/preamplifier was used to collect tdTomato fluorescence. Due to considerable bleed-through of the GCaMP signal into the tdTomato channel, we chose not to use the tdTomato recording trace to normalize our data, instead opting for a set of behavioural controls for motion artifacts (see below). The preamplifier output voltage signal was collected by a NIDAQ board (PCI-e6321, National Instruments) connected to a computer running LabVIEW (National Instruments) for signal acquisition. Video recordings were acquired at 15 frames per second and the signal from the optical fibre was sampled at 1 kHz. A TTL-triggered photodiode next to the cage was used to align videos and voltage recording traces.

Analysis was performed using custom Matlab (MathWorks) routines. Only recordings with a stable baseline were included in our analysis. The raw signal over each entire recording session was divided by the mean of a Gaussian fit to the distribution of GCaMP to normalize the baseline over the recording session. Since the increase in GCaMP signal preceded even detection in some cases (e.g. see Fig. 3c), Z-scores were calculated using the period −5 to −2 s prior to event detections as baseline and 0 to 3 s from event detection as signal. Statistical analyses (i.e. *t*-tests, ANOVA) considered a value of $p \leq 0.05$ significant. Behaviours were scored manually off-line by an experimenter blind to the photometry recording data. The responses to a stimulus type within a session (typically 5 – 10 trials per behaviour type) were averaged, and these session averages across mice were used as data displayed in Figures 3 and Extended Data Figure 6.

We performed a set of behavioural controls in order to address the possible contribution of motion artifacts to the recorded signal. In all of the following cases, (orofacial) motor actions highly identical to pup interactions did not result in detectable increases in GCaMP fluorescence intensity: (1) No increase in signal was observed when animals retrieved or sniffed a pup-sized cracker (Fig. 3j), during eating (Fig. 3k) or during self-grooming (Fig. 3l). In addition, (2) No increase in signal was detectable when animals retrieved bedding material to the nest (Fig. 3h), and (3) chemoinvestigation of accessible vs inaccessible pups resulted in different GCaMP responses (-5 to 0 s period before sniffing, Extended Data Fig. 6i, j). Therefore, the increases in signal intensity observed during pup interactions very likely represent actual activity changes rather than motion artifacts.

Optogenetics

Gal::Cre mice 8 – 12 weeks of age were used in these experiments. Since potential increases in parental behaviour would be difficult to detect in already highly parental mothers and fathers, we performed these experiments in virgin animals, in which a higher dynamic range of parental interactions can be assessed. Animals were exposed to two pups in their home cage (see 'Parental behaviour assay') and those that attacked (virgin males) or initiated parental behaviour (virgin females) within 15 min were selected for surgery. We injected 700 nl of AAV5/EF1α-DIO-hChR2(H134R)-EYFP (activation) or AAV5/EF1α-DIO-eNpHR3.0-EYFP (inhibition) bilaterally into the MPOA and in the same surgery a dual fibre – cannula (300 μm, 0.22 NA, Doric Lenses) was implanted 0.4 – 0.5 mm above the respective $MPOA^{Gal}$ projection target (Extended Data Table 1) and affixed to the skull with dental cement. Mice were tested 3 – 5 weeks after injection to allow for efficient expression of ChR2 or eNpHR3.0 into axon terminals. On testing day, the implant was connected to an optical fibre attached to either a 473 nm laser (150 mW, Laserglow Technologies) or a 460 nm LED (~50 W, Prizmatix) for optogenetic activation, or a 589 nm laser (300 mW, Opto Engine LLC) for inhibition, via a commutator. Animals were tested in either stimulation or non-stimulation trials in randomized order, with 2 d between trials. In addition, the order in which animals were tested during each experimental session was randomized. In pup exposure experiments, two *C57BL/6J* pups 1 – 3 d of age were introduced to the test animal's home cage in each corner furthest from the nest after 10 min of habituation. For activation experiments, blue light (473 nm) was delivered in 20-ms pulses at 20 Hz for 1 – 4 s whenever the animal contacted a pup with its snout. The light power exiting the fibre tip was 5 mW, which we calculated as providing an irradiance of 5 – 10 mW/mm^{-2} at the target region (using the brain tissue light transmission calculator provided by the Deisseroth laboratory, http://www.stanford.edu/group/dlab/cgi-bin/graph/chart.php). For loss-of-function experiments, constant yellow light (589 nm) was delivered at 8 – 10 mW at the fibre tip, amounting to an estimated irradiance of 15 – 20 mW/mm^{-2} at the target. Each trial lasted up to 10 min but when virgin males attacked and wounded a pup, the trial was ended and the pup was euthanized.

The following behaviours were scored and quantified: pup sniffing, -grooming and -licking, pup retrieval to the nest, aggression (animal grabs the pup violently and attempts to bite), crouching (animal hovers above the pup in the nest), nest building and time spent in the nest. For the motivation assay, following a 10 min habituation period a transparent barrier was inserted into the home cage, dividing the cage into a nest and a pup compartment. Next, 4 – 5 pups were introduced into the pup compartment and 473 nm light was delivered in 20-ms pulses at 20 Hz for 4 s every 10 s for a total of 6 min. Locomotion was assessed in a 36 × 25 cm arena over a period of 5 min. In stimulation trials, 473 nm light (20 ms, 20 Hz) was delivered to the implant for 4 s every 20 s, equivalent to the stimulation administered during a typical pup interaction trial. The position of the animal was tracked and analyzed by Ethovision XT 8 software (Noldus) to calculate the average velocity and moved distance. For intruder assays, an 8 – 12 week old *C57BL/6J* intruder of the opposite sex (receptive virgin female, as determined by vaginal smear, or sexually experienced male) was introduced into the resident mouse cage and 473 nm light was delivered in 20 ms pulses at 20 Hz for 1 – 4 s whenever the animal contacted the intruder with its snout. Sniffing and

grooming duration were scored over a period of 5 min, aggression was scored during a 10 min period. After behavioural testing, animals were transfused transcardially and fibre placement as well as efficient light transmission were verified.

Statistics and Reproducibility

Data were analysed either by two-tailed, unpaired or paired Student's *t*-test, by two-tailed Fisher's exact test or by Chi-square test if not indicated otherwise, using Graph Pad Prism 7 for Mac OS, Matlab or R. Statistical details are given in the respective figure legends. Experiments were independently performed twice (Fig. 1b–f, Fig. 2e–g, k, l, Fig. 3c–l, Fig. 4, Extended Data Fig. 1, Extended Data Fig. 2a–d, i, j, Extended Data Fig. 3d, e, Extended Data Fig. 4b–f, Extended Data Fig. 7, 8), three (Fig. 1g–j, Fig. 2b, c, h, I, Fig. 3n–p, Extended Data Fig. 6b–d) or four times (Extended Data Fig. 6f–h).

Data and code availability

The data and code that support the findings of this study are available from the corresponding author upon request.

Extended Data

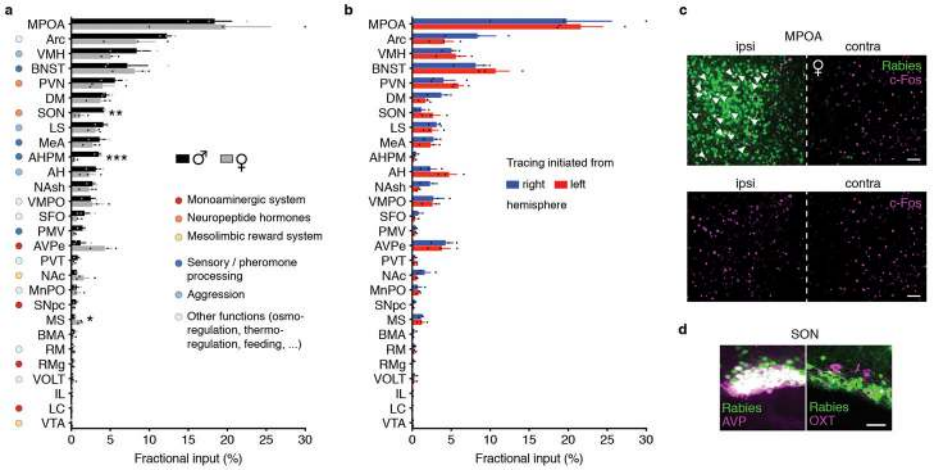

Extended Data Figure 1. Putative functional roles of brain areas providing monosynaptic inputs into MPOA^{Gal} neurons

a, Comparison between MPOA^{Gal} input fractions in virgin males (n = 3) and females (n = 3) after rabies tracing (see Fig. 2d). Sexually dimorphic inputs are highlighted. Two-tailed *t*-tests, SON: $^{**}P = 0.0041$, AHPM: $^{***}P = 0.0007$, MS: $^{*}P = 0.0133$. **b,** Comparison between MPOA^{Gal} input fractions after rabies tracing was initiated from the right (n = 3) or left (n = 3) hemisphere in virgin females. No significant differences were found ($P > 0.05$; two-tailed paired *t*-test). **c,** Comparison between rabies-injected (ipsilateral, ipsi) and non-injected (contralateral, contra) MPOA of a mother after parental behaviour. Activated (c-Fos^{+}) rabies^{+} neurons are shown (upper, arrowheads). c-Fos^{+} neuron numbers are not significantly different between hemispheres (lower, $P = 0.43$, 95% CI [−4.176, 1.843]; two-tailed paired *t*-test; n = 6). **d,** MPOA^{Gal} neurons receive monosynaptic inputs from magnocellular SON^{AVP} neurons (mothers, 72.7 ± 9.3% overlap, n = 3; virgin females, 77.4

± 4.3%, n = 3; fathers, 83.3 ± 3.3%, n = 3) but rarely from SON^{OXT} neurons (mothers, 4.6 ± 4.2% overlap, n = 2; virgin females, 4.5 ± 1.0%, n = 2; fathers, 2.8 ± 1.8%, n = 2). Scale bars, **c,** 100 μm; **d,** 50 μm. Data are mean ± s.e.m.

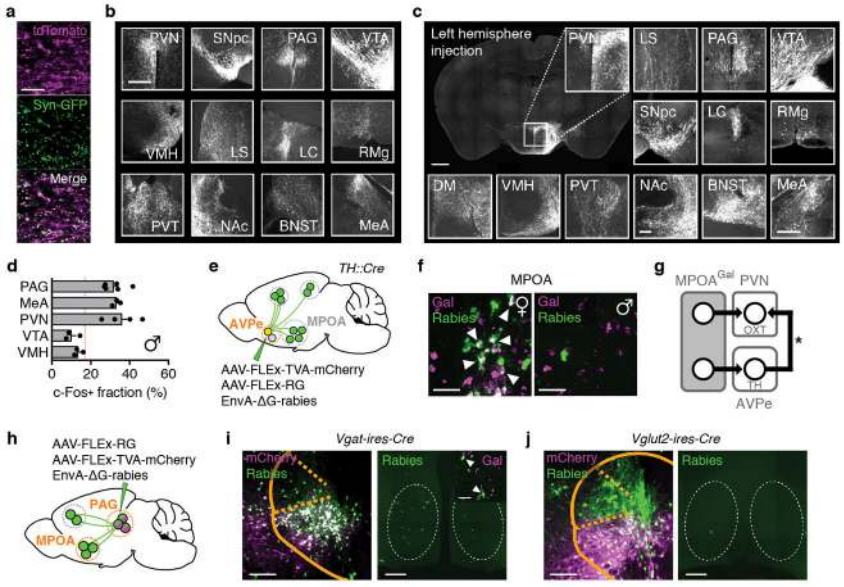

Extended Data Figure 2. $MPOA^{Gal}$ projections in males and downstream connectivity

a, Synaptophysin-GFP (Syn-GFP) labelling of presynaptic sites in $MPOA^{Gal}$ projections. **b,** Representative $MPOA^{Gal}$ projections from a virgin male, identified by tdTomato fluorescence. **c,** Representative $MPOA^{Gal}$ projections, identified by tdTomato fluorescence, after viral injection into the left MPOA. **d,** c-Fos^{+} fractions of virally labelled $MPOA^{Gal}$ projections in fathers (n = 6, 3, 4, 3, 3, respectively, from top). Red line depicts the population average (see ref. 3). Data are mean ± s.e.m. **e,** Trans-synaptic retrograde rabies tracing from $AVPe^{TH}$ neurons. **f,** $MPOA^{Gal}$ neurons presynaptic to $AVPe^{TH}$ neurons in females (left, arrowheads, 21.4% Gal^{+}, 47/220 neurons, n = 3) and males (right, 16.7% Gal^{+}, 4/24 neurons, n = 2). **g,** Direct and indirect $MPOA^{Gal} \rightarrow PVN^{OXT}$ connectivity. Asterisk, $AVPe^{TH}$ neurons form excitatory synapses with PVN^{OXT} in females[11]. **h,** Conditional monosynaptic retrograde tracing initiated from PAG. **i, j,** Injection sites with $mCherry^{+}$ starter neurons in PAG of *Vgat-ires-Cre* (**i,** left) or *Vglut2-ires-Cre* (**j,** left) mice. Presynaptic, $rabies^{+}/Gal^{+}$ neurons are detected in MPOA when tracing is initiated from PAG^{Vgat} (**i,** right, arrowheads), but not PAG^{Vglut2} (**j,** right), neurons. Scale bars, **a,** 50 μm; **b,** 250 μm; **c,** left, 500 and inset, 250 μm; **f,** 50 μm; **i, j,** left, 200 μm and right, 250 μm; **i,** insert**,** 50 μm.

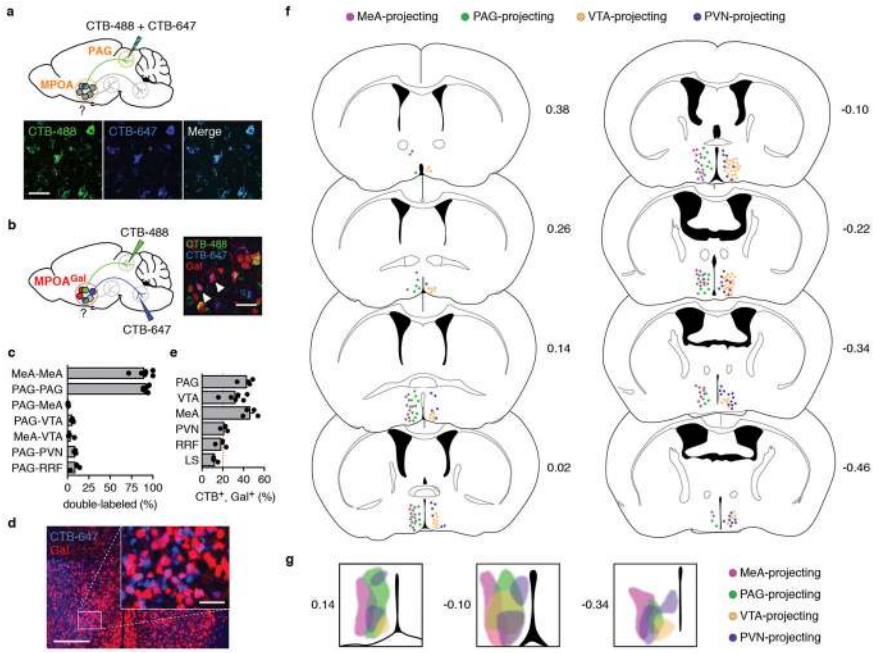

Extended Data Figure 3. MPOA^{Gal} projections correspond to largely non-overlapping neuronal subpopulations

a, Control injection of a 1:1 mixture of CTB-488 and CTB-647 into PAG results in highly overlapping neuron populations in the MPOA (quantification, see **c**). **b,** Strategy to determine collaterals between pairwise injected MPOA^{Gal} projections in *Gal::Cre*$^{+/-}$*; loxP-Stop-loxP-tdTomato*$^{+/-}$ mice. An example with two double-labelled MPOA^{Gal} neurons is shown after injection of CTB-488 into PAG and CTB-647 into VTA (right, arrowheads). **c,** Quantification of data in **a, b**. Data are mean ± s.e.m. (n = 6, 6, 3, 3, 3, 3, 3, respectively, from top). **d,** Representative image from MPOA of *Gal::Cre*$^{+/-}$*; loxP-Stop-loxP-tdTomato*$^{+/-}$ mouse after injection of CTB-647 into PAG. Note high overlap between Gal^{+} and CTB^{+} neurons. **e,** Frequency of Gal^{+} neurons in individual, CTB-labelled MPOA projections (n = 4, 6, 4, 3, 3, 3, respectively, from top). Red line depicts expected labelling frequency, based on proportion of Gal^{+} MPOA neurons (~20%, ref. 3). Data in **c, e** are mean ± s.e.m. **f,** Distribution of cell bodies corresponding to specific MPOA^{Gal} projections. Individual MPOA^{Gal} projection areas in *Gal::Cre* virgin females were injected with Cre-dependent CAV2-FLEx-ZsGreen (see Fig. 2h). Only labelling patterns on the ipsilateral, injected side are shown and only two projection-specific subpopulations per side are displayed for clarity. Distance from Bregma is shown in mm. Mouse brain images in this figure have been reproduced with permission from Elsevier[64]. **g,** Zones occupied by MPOA^{Gal} cell bodies projecting to MeA, PAG, VTA and PVN in anterior (left), central (middle) and posterior (right) MPOA. Distance from Bregma is shown in mm. Scale bars, **a, b,** 50 μm; **d,** 250 μm and inset, 50 μm.

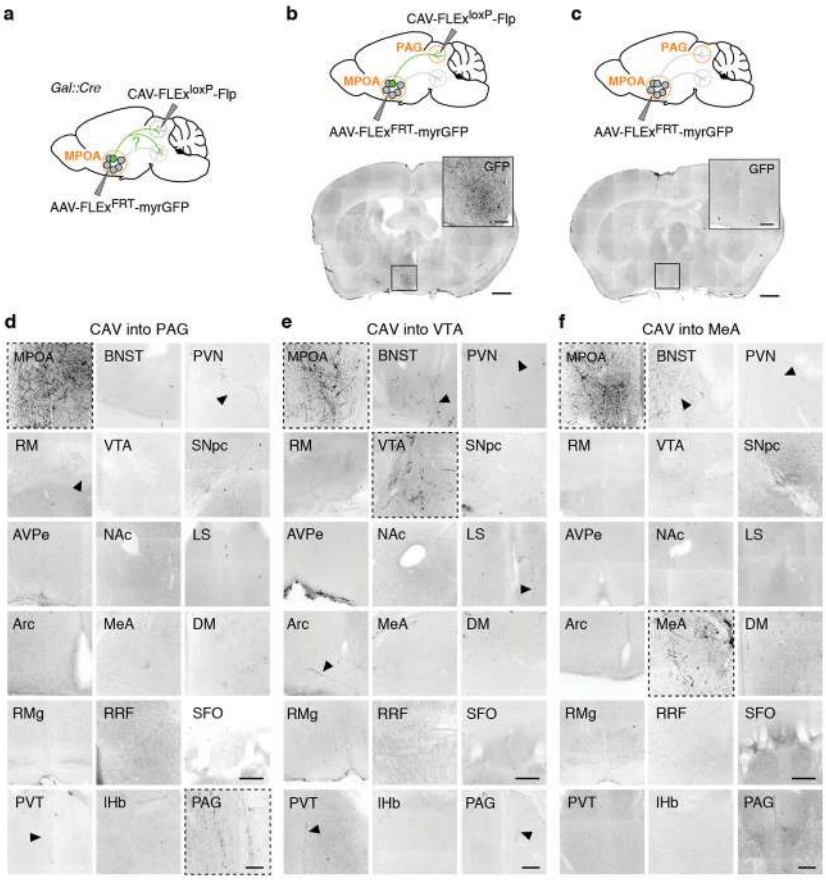

Extended Data Figure 4. MPOA^{Gal} projections barely collateralize

a, Strategy to detect brain-wide axon collaterals of specific MPOA^{Gal} projections. **b,** Dense labelling of MPOA^{Gal} neurons after injection of retrograde tracer CAV into PAG and reporter AAV into MPOA. **c,** Absence of MPOA^{Gal} labelling in negative control without injection of CAV. **d–f,** Only minor axon collaterals are detectable from MPOA^{Gal} neurons projecting to PAG (n = 2) (**d**), VTA (n = 3) (**e**) or MeA (n = 2) (**f**). Note MPOA→MeA fibre tract in BNST in (**f**). Signal was enhanced using anti-GFP immunostaining (Methods). Scale bars, **b, c,** 400 μm and insets, 100 μm; **d–f,** 150 μm.

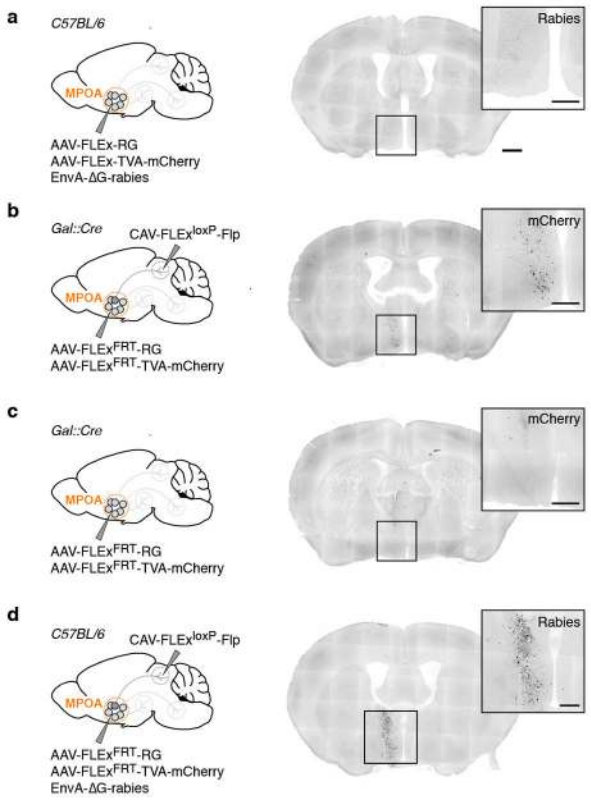

Extended Data Figure 5. Negative controls for monosynaptic retrograde tracing

a, Absence of rabies^{+} background labelling in the MPOA of AAV- and rabies-injected C57BL/6 control mice (n = 2). **b,** Labelling of MPOA^{Gal} neurons after injection of CAV into PAG and starter AAVs into MPOA of *Gal::Cre* mice (261 ± 19 neurons, n = 4). **c,** Near-absence of labelling in AAV-only negative control (11 ± 2 neurons, n = 2). **d,** Background rabies^{+} neurons were present in the following brain areas of CAV-, AAV- and rabies-injected C57BL/6 control mice (n = 3): MPOA, BNST, AH, PVN and SON. These areas were therefore excluded from analysis (see Figure 2k, l and Methods). Scale bars, **a–d,** 400 μm and insets, 150 μm.

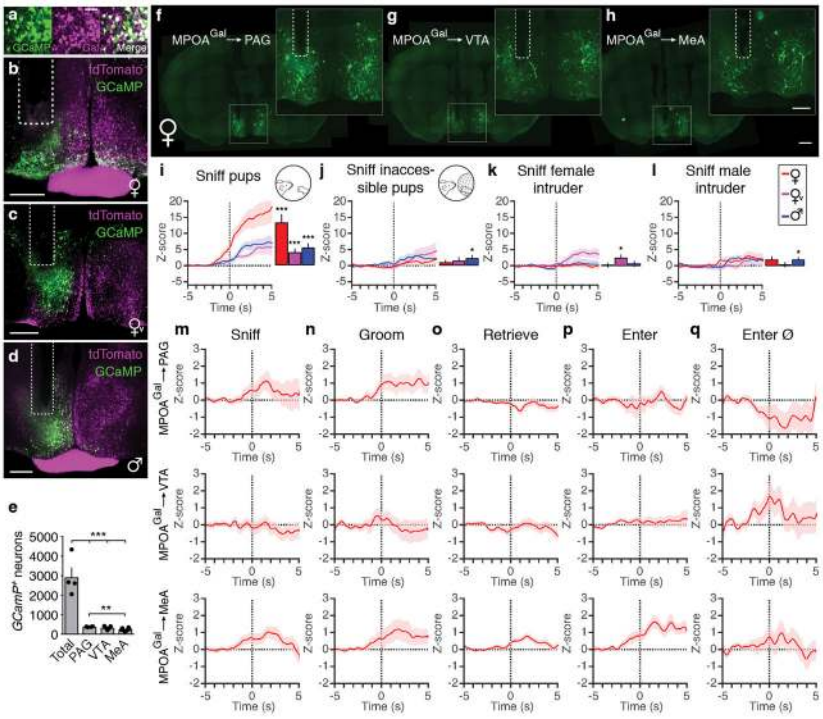

Extended Data Figure 6. Histology of photometry recording experiments and tuning of MPOA^{Gal} neurons in other behavioural contexts

a, Specific GCaMP6m expression in MPOA^{Gal} neurons (90.9 ± 4.3% overlap, n = 3, mothers). **b–d,** Implantation sites of optical fibres in the MPOA of *Gal::Cre$^{+/-}$; loxP-Stop-loxP-tdTomato$^{+/-}$* mother (**b**), virgin female (**c**) and father (**d**). **e,** Quantification of GCaMP^{+} neuron numbers in MPOA after AAV injection ('Total', n = 4) and after injection of HSV into individual projections (n = 5 each). Data for mothers are shown. Data are mean ± s.e.m. Two-tailed *t*-tests, Total vs. PAG, VTA, MeA: $***P < 0.001$, PAG vs. MeA: $**P = 0.0033$. **f–h,** Expression of GCaMP6m in MPOA^{Gal} neurons after bilateral infection of axon terminals in PAG (**f**), VTA (**g**) or MeA (**h**) with Cre-dependent, GCaMP6m-expressing HSV. Insets show fibre implantation sites. **i, j,** Averaged recording traces from MPOA^{Gal} neuron activity during sniffing of accessible pups (**i**) or inaccessible pups enclosed in a wire mesh tea ball (**j**) in mothers (n = 4), virgin females (n = 3) and fathers (n = 5). **k, l,** Averaged recording traces from MPOA^{Gal} neuron activity during sniffing of female (**k**) or male (**l**) intruder in mothers (n = 4), virgin females (n = 3) and fathers (n = 5). Two-tailed *t*-tests, **i**: $***P < 0.0001$, $***P < 0.0001$, $P = 0.0001$, **j**: $*P = 0.0380$, **k**: $*P = 0.0219$, **l**: $*P = 0.0272$. **m–q,** Averaged recording traces from MPOA^{Gal} neurons projecting to PAG (left, n = 10), VTA (middle, n = 12) or MeA (right, n = 8) during episodes of maternal behaviour. All traces and bar plots are mean ± s.e.m. Scale bars, **a,** 50 μm; **b–d,** 400 μm; **f–h,** 1 mm and insets, 500 μm.

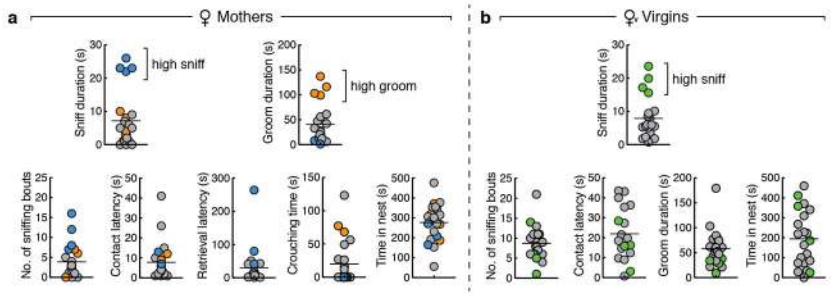

Extended Data Figure 7. Distribution of parental behaviours in mothers and virgin females

Distribution of parental behaviours during 10 min pup interaction assays in mothers (**a,** n = 23) and virgin females (**b,** n = 20). In **a,** individuals exhibiting high pup sniffing are indicated in blue across plots, and individuals exhibiting high pup grooming are indicated in orange. In **b,** individuals exhibiting high pup sniffing are indicated in green. Note that *y* axis ranges are identical between **a** and **b**. Lines depict mean.

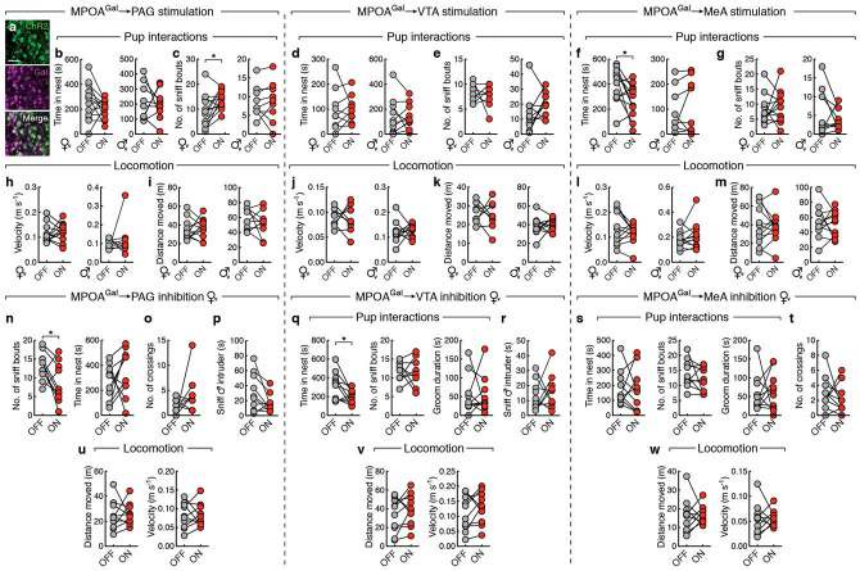

Extended Data Figure 8. Behavioural specificity of MPOA^{Gal} projection stimulation

a, Channelrhodopsin-2 (ChR2) expression in MPOA^{Gal} neurons (97.7 ± 0.2% overlap, virgin female, n = 2). **b–g,** Effect of activating PAG- (**b, c**), VTA- (**d, e**) or MeA- (**f, g**) projections on time spent in nest in females and males (**b,** n = 13, 10; **d,** n = 9, 10; **f,** n = 10, 10) and number of pup-directed sniffing bouts (**c,** n = 13, 10; **e,** n = 9, 10**; g,** n = 10, 10). **h–m,** Effect of activating PAG- (**h, i**), VTA- (**j, k**) or MeA- (**l, m**) projections on locomotion velocity (**h,** n = 13, 10; **j,** n = 8, 10; **l,** n = 10, 10) and moved distance (**i, k, m**). **n, q, s,** Effect of inhibiting PAG- (**n,** n = 10), VTA- (**q,** n = 10) or MeA- (**s,** n = 11) projections on pup interactions. **o, t,** Effect of inhibiting PAG- (**o,** n = 10) or MeA- (**t,** n = 11) projections on number of barrier crosses. **p, r,** Effect of inhibiting PAG- (**p,** n = 10) or MeA- (**r,** n = 11) projections on chemoinvestigation of a male intruder. **u–w,** Effect of inhibiting PAG- (**u**), VTA- (**v**) or MeA- (**w**) projections on locomotion velocity and moved distance (n = 10, 10,

11, respectively). Two-tailed paired *t*-tests, **c:** **P* = 0.0135, **f:** **P* = 0.03, **n:** **P* = 0.0413, **q:** **P* = 0.0264. Scale bar in **a,** 50 μm.

Extended Data Table 1

List of brain areas and coordinates (Note: no table legend)

Abbreviation	Brain area	Injection coord. (AP/ML/DV)	Stimulation coord. (AP/ML/DV)	Recording coor
AH	anterior hypothalamus	–	–	
AHPM	posteriomedial amygdalohippocampal area	–	–	
Arc	arcuate nucleus	–	–	
AVPe	anteroventral periventricular nucleus	0.25/0.15/−5.45	–	
BMA	basomedial amygdala	–	–	
BNST	bed nucleus of the stria terminalis	–	–	
DM	dorsomedial hypothalamus	–	–	
IL	infralimbic cortex	–	–	
LC	locus coeruleus	−5.4/0.88/−2.65	–	
LS	lateral septum	0.4/0.3/−2.5	–	
MeA	medial amygdala	−1.6/2.25/−4.95	−1.6/±2.25/−4.5	
MnPO	median preoptic nucleus	–	–	
MPOA	medial preoptic area	0/0.5/−5.05	–	0/0.5
MS	medial septum	–	–	
NAc	nucleus accumbens - core	1.0/0.7/−3.8	–	
NAsh	nucleus accumbens - shell	–	–	
PAG	(rostral) periaqueductal grey	−3.28/0.2/−2.5	−3.28/±0.2/−2.2	
PeFA	perifornical area	−0.6/0.3/−4.2	–	
PMV	ventral premammillary nucleus	–	–	
PVN	periventricular hypothalamic nucleus	−0.82/0.25/−4.6	–	
PVT	periventricular thalamic nucleus	−0.94/0/−2.7	–	
RM	retromammillary nucleus	–	–	
RRF	retrorubral field	−4.04/1.0/−3.4	–	
RMg	raphe magnus nucleus	−5.2/0/−4.55	–	
SFO	subfornical organ	–	–	
SNpc	substantia nigra pars compacta	−3.1/1.25/−4.0	–	
SON	supraoptic nucleus	–	–	
VMH	ventromedial hypothalamus	−1.5/0.4/−5.7	–	
VOLT	vascular organ of the lamina terminalis	–	–	
VTA	ventral tegmental area	−3.0/0.6/−4.2	−3.1/±0.5/−4.1	

Extended Data Table 2
Summary of parenting-affecting manipulations in MPOA^{Gal} target areas

From those brain areas targeted by MPOA^{Gal} projections (Fig. 2c), manipulation of the following has been shown to affect maternal behaviour in rats (or mice where indicated). For a more comprehensive review see ref. 10.

Brain area	Manipulation	Effect	Reference
PAG	Lesion	Facilitates maternal responses	44
	$GABA_A$ receptor antagonist	Decreases maternal aggression, Increases pup licking/grooming	19
MeA	Lesion	Accelerates onset of maternal behaviour	45–47
PVN	Lesion	Disrupts onset of maternal behaviour	48 (but see 49)
LS	$GABA_A$ receptor antagonist	Decreases maternal aggression	50
	Corticotropin releasing factor	Decreases maternal aggression	51
LC	Disruption of 5-HT production	Disrupts maternal behaviour (mice)	51
AVPe	Ablation of TH^+ neurons	Impairs maternal behaviour (mice)	11
	Optogenetic stimulation of TH^+ neurons	Enhances maternal behaviour (mice)	
VTA	Lesion	Impairs pup retrieval	2,52
	Inactivation	Impairs pup-paired conditioned place preference	22
NAc	Lesion	Impairs pup retrieval	53,54
	DA receptor antagonist	Inhibits retrieval and licking; enhances nursing	55,56
SNpc	Lesion	Disrupts maternal behaviour	57
VMH	Lesion	Accelerates onset of maternal behaviour	58
BNST	Lesion (ventral BNST)	Disrupts maternal behaviour	59
	Estrogen injection	Facilitates maternal responses	60
	Prolactin injection	Facilitates maternal responses	61
RRF	n/a	RRF-projecting lVIPOA neurons activated during maternal behaviour	62
PVT	n/a	Activated during maternal behaviour	63

Supplementary Material

Refer to Web version on PubMed Central for supplementary material.

Acknowledgments

We thank S. Sullivan for help with behaviour and mouse husbandry. E. Kremer (Montpellier) and R. Neve (MIT) provided viral vectors. E. Soucy and J. Greenwood helped design motivation assay. R. Hellmiss and K. Wilbur helped with illustrations. H.S. Knobloch-Bollmann provided advice on PVN cell types. We thank members of the Dulac lab for comments on the manuscript. This work was supported by a Human Frontier Long-Term Fellowship, an EMBO Long-Term Fellowship and a Sir Henry Wellcome Fellowship to J.K., Fondation pour la Recherche Médicale grant SPE20150331860 to B.M.B., a NIH K99 Award and a NARSAD Young Investigator Award to A.E.A., a Howard Hughes Gilliam Fellowship to B.M.B., a Harvard Mind Brain and Behavior faculty grant to N.U. and NIH grant 1R01HD082131-01A1 to C.D. C.D. and L.L. are investigators of the Howard Hughes Medical Institute.

Main text references

1. Dulac C, O'Connell LA, Wu Z. Neural control of maternal and paternal behaviors. Science. 2014; 345:765–770. DOI: 10.1126/science.1253291 [PubMed: 25124430]
2. Numan, M., Insel, TR. The neurobiology of parental behavior. Springer; 2011.
3. Wu Z, Autry AE, Bergan JF, Watabe-Uchida M, Dulac CG. Galanin neurons in the medial preoptic area govern parental behaviour. Nature. 2014; 509:325–330. DOI: 10.1038/nature13307 [PubMed: 24828191]
4. Wickersham IR, et al. Monosynaptic restriction of transsynaptic tracing from single, genetically targeted neurons. Neuron. 2007; 53:639–647. DOI: 10.1016/j.neuron.2007.01.033 [PubMed: 17329205]
5. Marlin BJ, Mitre M, D'Amour JA, Chao MV, Froemke RC. Oxytocin enables maternal behaviour by balancing cortical inhibition. Nature. 2015; 520:499–504. DOI: 10.1038/nature14402 [PubMed: 25874674]
6. Johnson ZV, Young LJ. Oxytocin and vasopressin neural networks: Implications for social behavioral diversity and translational neuroscience. Neurosci Biobehav Rev. 2017; 76:87–98. DOI: 10.1016/j.neubiorev.2017.01.034 [PubMed: 28434591]
7. Bendesky A, et al. The genetic basis of parental care evolution in monogamous mice. Nature. 2017
8. Tachikawa KS, Yoshihara Y, Kuroda KO. Behavioral transition from attack to parenting in male mice: a crucial role of the vomeronasal system. J Neurosci. 2013; 33:5120–5126. DOI: 10.1523/JNEUROSCI.2364-12.2013 [PubMed: 23516278]
9. vom Saal FS. Time-contingent change in infanticide and parental behavior induced by ejaculation in male mice. Physiol Behav. 1985; 34:7–15. [PubMed: 4041052]
10. Kohl J, Autry AE, Dulac C. The neurobiology of parenting: A neural circuit perspective. Bioessays. 2017; 39:1–11. DOI: 10.1002/bies.201600159
11. Scott N, Prigge M, Yizhar O, Kimchi T. A sexually dimorphic hypothalamic circuit controls maternal care and oxytocin secretion. Nature. 2015; 525:519–522. DOI: 10.1038/nature15378 [PubMed: 26375004]
12. Schwarz LA, et al. Viral-genetic tracing of the input-output organization of a central noradrenaline circuit. Nature. 2015; 524:88–92. DOI: 10.1038/nature14600 [PubMed: 26131933]
13. Gunaydin LA, et al. Natural neural projection dynamics underlying social behavior. Cell. 2014; 157:1535–1551. DOI: 10.1016/j.cell.2014.05.017 [PubMed: 24949967]
14. Kudo Y, et al. A single optical fiber fluorometric device for measurement of intracellular Ca2+ concentration: its application to hippocampal neurons in vitro and in vivo. Neuroscience. 1992; 50:619–625. [PubMed: 1436506]
15. Elyada YM, Mizrahi A. Becoming a mother-circuit plasticity underlying maternal behavior. Curr Opin Neurobiol. 2015; 35:49–56. DOI: 10.1016/j.conb.2015.06.007 [PubMed: 26143475]
16. Andermann ML, Lowell BB. Toward a Wiring Diagram Understanding of Appetite Control. Neuron. 2017; 95:757–778. DOI: 10.1016/j.neuron.2017.06.014 [PubMed: 28817798]
17. Li Y, et al. Neuronal Representation of Social Information in the Medial Amygdala of Awake Behaving Mice. Cell. 2017; 171:1176–1190 e1117. DOI: 10.1016/j.cell.2017.10.015 [PubMed: 29107332]
18. Remedios R, et al. Social behaviour shapes hypothalamic neural ensemble representations of conspecific sex. Nature. 2017; 550:388–392. DOI: 10.1038/nature23885 [PubMed: 29052632]
19. Lee G, Gammie SC. GABAA receptor signaling in caudal periaqueductal gray regulates maternal aggression and maternal care in mice. Behav Brain Res. 2010; 213:230–237. DOI: 10.1016/j.bbr.2010.05.001 [PubMed: 20457185]
20. Salamone JD, Correa M. The mysterious motivational functions of mesolimbic dopamine. Neuron. 2012; 76:470–485. DOI: 10.1016/j.neuron.2012.10.021 [PubMed: 23141060]
21. McHenry JA, et al. Hormonal gain control of a medial preoptic area social reward circuit. Nat Neurosci. 2017; 20:449–458. DOI: 10.1038/nn.4487 [PubMed: 28135243]

22. Seip KM, Morrell JI. Transient inactivation of the ventral tegmental area selectively disrupts the expression of conditioned place preference for pup- but not cocaine-paired contexts. Behav Neurosci. 2009; 123:1325–1338. DOI: 10.1037/a0017666 [PubMed: 20001116]
23. Qualls-Creekmore E, et al. Galanin-Expressing GABA Neurons in the Lateral Hypothalamus Modulate Food Reward and Noncompulsive Locomotion. J Neurosci. 2017; 37:6053–6065. DOI: 10.1523/JNEUROSCI.0155-17.2017 [PubMed: 28539422]
24. Isogai Y, et al. Molecular organization of vomeronasal chemoreception. Nature. 2011; 478:241–245. DOI: 10.1038/nature10437 [PubMed: 21937988]
25. Bergan JF, Ben-Shaul Y, Dulac C. Sex-specific processing of social cues in the medial amygdala. Elife. 2014; 3:e02743. [PubMed: 24894465]
26. Yao S, Bergan J, Lanjuin A, Dulac C. Oxytocin signaling in the medial amygdala is required for sex discrimination of social cues. Elife. 2017; 6
27. Hong W, Kim DW, Anderson DJ. Antagonistic control of social versus repetitive self-grooming behaviors by separable amygdala neuronal subsets. Cell. 2014; 158:1348–1361. DOI: 10.1016/j.cell.2014.07.049 [PubMed: 25215491]
28. Anderson DJ. Circuit modules linking internal states and social behaviour in flies and mice. Nat Rev Neurosci. 2016; 17:692–704. DOI: 10.1038/nrn.2016.125 [PubMed: 27752072]
29. Yang T, Shah NM. Molecular and neural control of sexually dimorphic social behaviors. Curr Opin Neurobiol. 2016; 38:89–95. DOI: 10.1016/j.conb.2016.04.015 [PubMed: 27162162]
30. Zimmerman CA, Leib DE, Knight ZA. Neural circuits underlying thirst and fluid homeostasis. Nat Rev Neurosci. 2017; 18:459–469. DOI: 10.1038/nrn.2017.71 [PubMed: 28638120]
31. Weber F, Dan Y. Circuit-based interrogation of sleep control. Nature. 2016; 538:51–59. DOI: 10.1038/nature19773 [PubMed: 27708309]
32. Arber S. Motor circuits in action: specification, connectivity, and function. Neuron. 2012; 74:975–989. DOI: 10.1016/j.neuron.2012.05.011 [PubMed: 22726829]
33. Madisen L, et al. A robust and high-throughput Cre reporting and characterization system for the whole mouse brain. Nat Neurosci. 2010; 13:133–140. DOI: 10.1038/nn.2467 [PubMed: 20023653]
34. Miyamichi K, et al. Dissecting local circuits: parvalbumin interneurons underlie broad feedback control of olfactory bulb output. Neuron. 2013; 80:1232–1245. DOI: 10.1016/j.neuron.2013.08.027 [PubMed: 24239125]
35. Beier KT, et al. Circuit Architecture of VTA Dopamine Neurons Revealed by Systematic Input-Output Mapping. Cell. 2015; 162:622–634. DOI: 10.1016/j.cell.2015.07.015 [PubMed: 26232228]
36. Esposito MS, Capelli P, Arber S. Brainstem nucleus MdV mediates skilled forelimb motor tasks. Nature. 2014; 508:351–356. DOI: 10.1038/nature13023 [PubMed: 24487621]
37. Eliava M, et al. A New Population of Parvocellular Oxytocin Neurons Controlling Magnocellular Neuron Activity and Inflammatory Pain Processing. Neuron. 2016; 89:1291–1304. DOI: 10.1016/j.neuron.2016.01.041 [PubMed: 26948889]
38. Xiao L, Priest MF, Nasenbeny J, Lu T, Kozorovitskiy Y. Biased Oxytocinergic Modulation of Midbrain Dopamine Systems. Neuron. 2017; 95:368–384 e365. DOI: 10.1016/j.neuron.2017.06.003 [PubMed: 28669546]
39. Swanson LW, Sawchenko PE. Hypothalamic integration: organization of the paraventricular and supraoptic nuclei. Annu Rev Neurosci. 1983; 6:269–324. DOI: 10.1146/annurev.ne.06.030183.001413 [PubMed: 6132586]
40. Wickersham IR, Finke S, Conzelmann KK, Callaway EM. Retrograde neuronal tracing with a deletion-mutant rabies virus. Nat Methods. 2007; 4:47–49. DOI: 10.1038/nmeth999 [PubMed: 17179932]
41. Osakada F, et al. New rabies virus variants for monitoring and manipulating activity and gene expression in defined neural circuits. Neuron. 2011; 71:617–631. DOI: 10.1016/j.neuron.2011.07.005 [PubMed: 21867879]
42. Weible AP, et al. Transgenic targeting of recombinant rabies virus reveals monosynaptic connectivity of specific neurons. J Neurosci. 2010; 30:16509–16513. DOI: 10.1523/JNEUROSCI.2442-10.2010 [PubMed: 21147990]
43. Menegas W, Babayan BM, Uchida N, Watabe-Uchida M. Opposite initialization to novel cues in dopamine signaling in ventral and posterior striatum in mice. Elife. 2017; 6

44. Sukikara MH, Mota-Ortiz SR, Baldo MV, Felicio LF, Canteras NS. The periaqueductal gray and its potential role in maternal behavior inhibition in response to predatory threats. Behav Brain Res. 2010; 209:226–233. DOI: 10.1016/j.bbr.2010.01.048 [PubMed: 20138922]
45. Fleming AS, Vaccarino F, Luebke C. Amygdaloid inhibition of maternal behavior in the nulliparous female rat. Physiol Behav. 1980; 25:731–743. [PubMed: 7443835]
46. Numan M, Numan MJ, English JB. Excitotoxic amino acid injections into the medial amygdala facilitate maternal behavior in virgin female rats. Horm Behav. 1993; 27:56–81. DOI: 10.1006/hbeh.1993.1005 [PubMed: 8440518]
47. Sheehan T, Paul M, Amaral E, Numan MJ, Numan M. Evidence that the medial amygdala projects to the anterior/ventromedial hypothalamic nuclei to inhibit maternal behavior in rats. Neuroscience. 2001; 106:341–356. [PubMed: 11566505]
48. Insel TR, Harbaugh CR. Lesions of the hypothalamic paraventricular nucleus disrupt the initiation of maternal behavior. Physiol Behav. 1989; 45:1033–1041. [PubMed: 2780864]
49. Numan M, Corodimas KP. The effects of paraventricular hypothalamic lesions on maternal behavior in rats. Physiol Behav. 1985; 35:417–425. [PubMed: 2999841]
50. Lee G, Gammie SC. GABA(A) receptor signaling in the lateral septum regulates maternal aggression in mice. Behav Neurosci. 2009; 123:1169–1177. DOI: 10.1037/a0017535 [PubMed: 20001101]
51. D'Anna KL, Gammie SC. Activation of corticotropin-releasing factor receptor 2 in lateral septum negatively regulates maternal defense. Behav Neurosci. 2009; 123:356–368. DOI: 10.1037/a0014987 [PubMed: 19331459]
52. Hansen S, Harthon C, Wallin E, Lofberg L, Svensson K. Mesotelencephalic dopamine system and reproductive behavior in the female rat: effects of ventral tegmental 6-hydroxydopamine lesions on maternal and sexual responsiveness. Behav Neurosci. 1991; 105:588–598. [PubMed: 1930726]
53. Hansen S. Maternal behavior of female rats with 6-OHDA lesions in the ventral striatum: characterization of the pup retrieval deficit. Physiol Behav. 1994; 55:615–620. [PubMed: 8190785]
54. Li M, Fleming AS. The nucleus accumbens shell is critical for normal expression of pup-retrieval in postpartum female rats. Behav Brain Res. 2003; 145:99–111. [PubMed: 14529809]
55. Keer SE, Stern JM. Dopamine receptor blockade in the nucleus accumbens inhibits maternal retrieval and licking, but enhances nursing behavior in lactating rats. Physiol Behav. 1999; 67:659–669. [PubMed: 10604835]
56. Numan M, et al. The effects of D1 or D2 dopamine receptor antagonism in the medial preoptic area, ventral pallidum, or nucleus accumbens on the maternal retrieval response and other aspects of maternal behavior in rats. Behav Neurosci. 2005; 119:1588–1604. DOI: 10.1037/0735-7044.119.6.1588 [PubMed: 16420162]
57. Numan M, Nagle DS. Preoptic area and substantia nigra interact in the control of maternal behavior in the rat. Behav Neurosci. 1983; 97:120–139. [PubMed: 6682333]
58. Bridges RS, Mann PE, Coppeta JS. Hypothalamic involvement in the regulation of maternal behaviour in the rat: inhibitory roles for the ventromedial hypothalamus and the dorsal/anterior hypothalamic areas. J Neuroendocrinol. 1999; 11:259–266. [PubMed: 10223279]
59. Numan M, Numan M. A lesion and neuroanatomical tract-tracing analysis of the role of the bed nucleus of the stria terminalis in retrieval behavior and other aspects of maternal responsiveness in rats. Dev Psychobiol. 1996; 29:23–51. [PubMed: 8719181]
60. Numan M, Rosenblatt JS, Komisaruk BR. Medial preoptic area and onset of maternal behavior in the rat. J Comp Physiol Psychol. 1977; 91:146–164. [PubMed: 402400]
61. Bridges RS, Numan M, Ronsheim PM, Mann PE, Lupini CE. Central prolactin infusions stimulate maternal behavior in steroid-treated, nulliparous female rats. Proc Natl Acad Sci U S A. 1990; 87:8003–8007. [PubMed: 2236014]
62. Numan M, Numan MJ. Projection sites of medial preoptic area and ventral bed nucleus of the stria terminalis neurons that express Fos during maternal behavior in female rats. J Neuroendocrinol. 1997; 9:369–384. [PubMed: 9181491]
63. Lonstein JS, Simmons DA, Swann JM, Stern JM. Forebrain expression of c-fos due to active maternal behaviour in lactating rats. Neuroscience. 1998; 82:267–281. [PubMed: 9483519]

64. Franklin, KBJ., Paxinos, G. The Mouse Brain in Stereotaxic Coordinates. 3. Academic Press; 2007.

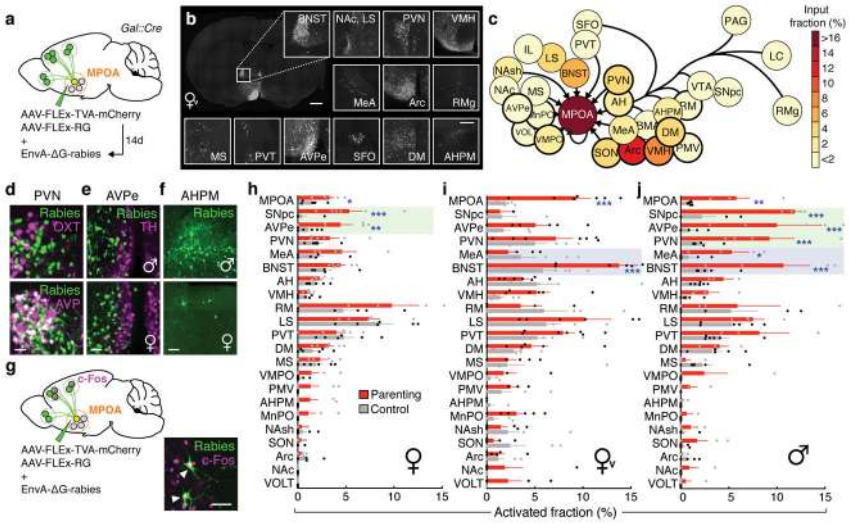

Figure 1. MPOA^{Gal} inputs are activated during parental behaviour in a sex- and reproductive state-specific manner

a, Monosynaptic retrograde tracing from MPOA^{Gal} neurons. **b,** Input areas with rabies^{+} neurons. **c,** Overview of inputs into MPOA^{Gal} neurons. Hypothalamic input areas in bold. **d,** MPOA^{Gal} neurons receive monosynaptic inputs from magnocellular PVN^{AVP} (37.6 ± 4.1% overlap, n = 3) but rarely PVN^{OXT} (2.6 ± 0.6%, n = 3) neurons. **e,** Presynaptic neurons in AVPe are TH^{-} in males (1.9% TH^{+}, n = 2) and females (1.8% TH^{+}, n = 3). **f,** Presynaptic neurons in AHPM. **g,** Identification of activated MPOA^{Gal} inputs and example of c-Fos^{+} presynaptic neurons. **h–j,** Activated input fractions in mothers (**h**), virgin females (**i**) and fathers (**j**) (each n = 6, controls n = 6). Green boxes, parent-specific activation, blue boxes, father- and virgin female-specific activation. Two-tailed *t*-tests (corrected for multiple comparisons, Methods), **h**: $***P < 0.0001$, $**P = 0.0267$, $*P = 0.0196$, **i**: $***P < 0.0001$, **j**: $***P < 0.0001$, $**P = 0.0035$, $*P = 0.0104$. Data in **h–j** are mean ± s.e.m. *n* = number of animals in all figures. Scale bars, **b,** left, 500 μm, inset, 250 μm; **d–g,** 50 μm. Abbreviations, see Extended Data Table 1.

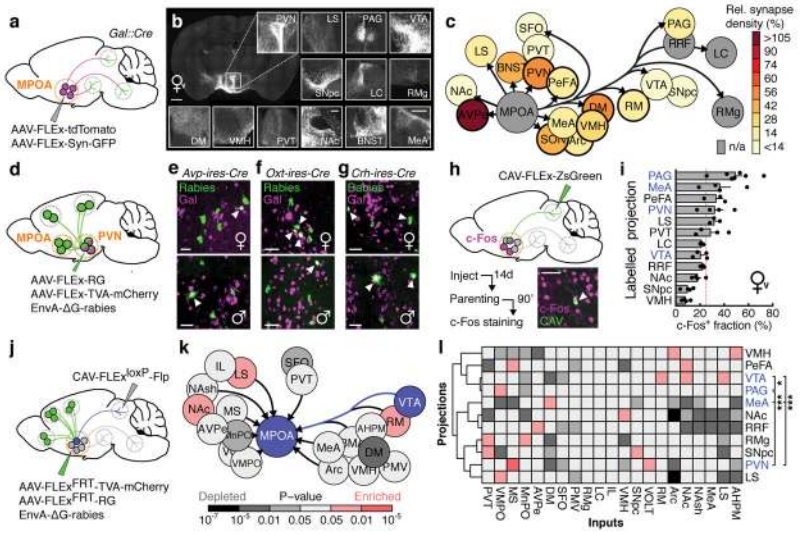

Figure 2. Identification of parenting-activated MPOA^{Gal} projections and input-output logic of the MPOA^{Gal} circuit

a, Visualisation of MPOA^{Gal} projections. **b,** MPOA^{Gal} projections identified by tdTomato fluorescence. **c,** Relative synaptic density in MPOA^{Gal} projection targets (n = 4, Methods). Grey regions could not be quantified due to tissue autofluorescence. Hypothalamic target areas in bold. **d,** Monosynaptic retrograde tracing from PVN. **e–g,** MPOA^{Gal} neurons presynaptic to (**e**) PVN^{AVP} (female 15/364 Gal^{+}, n = 3; male 46/180 Gal^{+}, n = 3) to (**f**) PVN^{OXT} (female 26/71 Gal^{+}, n = 3; male 7/51 Gal^{+}, n = 3) and to (**g**) PVN^{CRH} neurons (female 19/72 Gal^{+}, n = 3; male 22/45 Gal^{+}, n = 3). Significantly more MPOA neurons presynaptic to PVN^{AVP} and PVN^{CRH} were Gal^{+} in males than in females ($P < 0.0001$, $P =$ 0.0170, two-tailed Fisher's exact test) whereas more MPOA neurons presynaptic to PVN^{OXT} were Gal^{+} in females than in males ($P = 0.0068$). **h,** Labelling strategy for MPOA^{Gal} projections; example of retrogradely labelled c-Fos^{+} neuron in the MPOA. **i,** Activated fraction of MPOA^{Gal} neurons projecting to parenting-relevant brain areas (n = 7, 4, 3, 4, 3, 4, 3, 4, 3, 4, 4, 4, from top). Data are mean ± s.e.m. Red line, population average (ref. 3). Projections chosen for further functional studies are highlighted. **j,** Strategy for monosynaptic retrograde tracing from projection-defined MPOA^{Gal} subpopulations. **k, l,** Map of monosynaptic inputs into VTA-projecting MPOA^{Gal} neurons (**k**) and matrix displaying inputs into projection-defined MPOA^{Gal} subpopulations (**l,** Methods; n = 5, 3, 4, 4, 4, 4, 5, 5, 4, 4, 3, from top). Tukey post-hoc test assessed whether candidate projections (blue) receive quantitatively different inputs; VTA vs. PAG: $*P = 0.0205$, PAG vs. PVN: $***P = 0.0002$, all other comparisons: $***P < 0.0001$. Scale bars, **b,** left, 500 and inset, 250 μm; **e–g, h,** 50 μm.

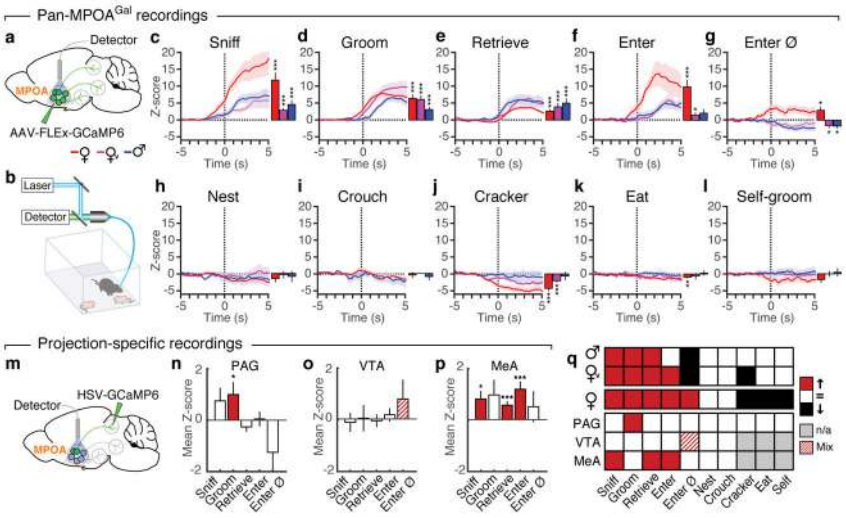

Figure 3. Distinct projection-defined MPOA^{Gal} neuronal pools are tuned to specific aspects of parental behaviour

a, b, Fibre photometry recording strategy (**a**) and setup (**b**). **c–i,** Averaged recording traces from MPOA^{Gal} population activity during pup sniffing (**c**), -grooming (**d**), -retrieval (**e**), entering nest with pups (**f**), entering empty nest (**g**), nest building (**h**) and crouching (**i**). Mean peak activity (Z-scores) shown in mothers (n = 4), virgin females (n = 3) and fathers (n = 5). **j–l,** Averaged recording traces and mean peak activity during control behaviours. **m,** Strategy for recording projection-defined MPOA^{Gal} subpopulations. **n–p,** Mean peak activation for PAG- (**n,** n = 10), VTA- (**o,** n = 12) and MeA- (**p,** n = 8) projections during parenting. **q,** Tuning matrix for pan-MPOA^{Gal} (upper) and projection-specific (lower) recordings. Two-tailed t-tests (Methods), **c**: $***P < 0.0001$, $***P < 0.0001$, $P = 0.0001$, **d**: $***P < 0.0001$, **e**: $***P < 0.0001$, $***P = 0.0008, 0.0004$, **f**: $***P < 0.0001$, $*P = 0.0247$, **g**: $*P = 0.0185, 0.0365, 0.0105$, **j**: $***P = 0.0002$, $***P < 0.0001$, **k**: $**P = 0.0059$, **n**: $*P = 0.0362$, **p**: $*P = 0.0102$, $***P < 0.0001$, $***P = 0.0001$. Data are mean ± s.e.m.

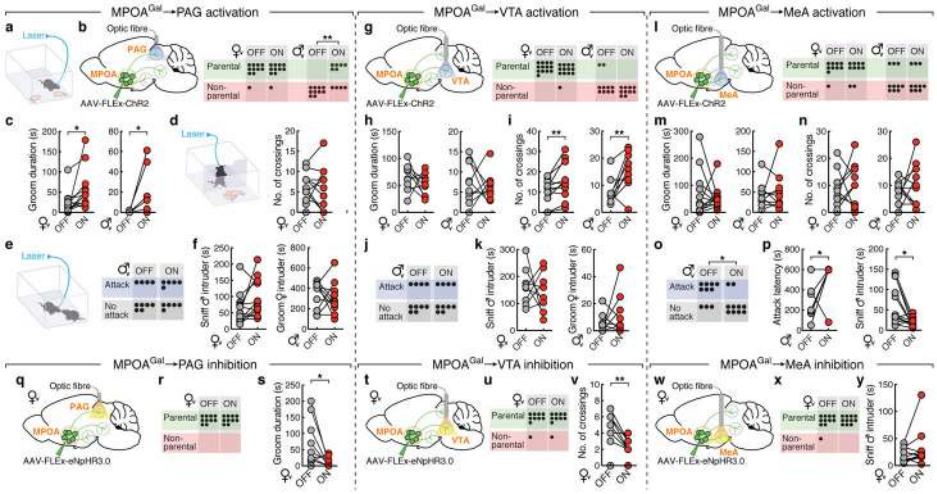

Figure 4. MPOA^{Gal} projections mediate discrete aspects of parental behaviour

a, Setup for optogenetic manipulations. **b, g, l,** Activation of MPOA^{Gal} projections (left); pup-directed behaviour in virgin females and males without ('OFF') or with ('ON') activation of PAG- (**b**), VTA- (**g**) and MeA- (**l**) projections. **c, h, m,** Effect of activating PAG- (**c**), VTA- (**h**) or MeA- (**m**) projections on pup grooming (virgin females, n = 13, 9, 10; males, n = 9, 10, 10). **d, i, n,** Motivation assay (**d**) and effect of activating PAG- (**d**), VTA- (**i**) or MeA- (**n**) projections on barrier crossing (virgin females, n = 13, 10, 10; males, n = 13, 10). **e, j, o,** Intruder assay (**e**) and effect of activating PAG- (**e**), VTA- (**j**) or MeA- (**o**) projections on male-male aggression. **f, k,** Effect of MPOA^{Gal}→PAG (**f**) or MPOA^{Gal}→VTA (**k**) activation on male- (n = 12, 9) or female-directed (n = 10, 10) behaviour. **p,** Effect of MPOA^{Gal}→MeA activation on male-directed attack latency (n = 10) and chemoinvestigation (n = 10). **q, t, w,** Inhibition of MPOA^{Gal} projections. **r, u, x,** Pup-directed behaviour in virgin females without ('OFF') or with ('ON') inhibition of PAG- (**r,** n = 10), VTA- (**u,** n = 10) and MeA- (**x,** n = 11) projections. **s,** Effect of MPOA^{Gal}→PAG inhibition on pup grooming (n = 10). **v,** Effect of MPOA^{Gal}→VTA inhibition on barrier crossing (n = 10). **y,** Effect of MPOA^{Gal}→MeA inhibition male-directed chemoinvestigation (n = 11). Chi-square (**b, e, g, j, l, o, r, u, x**) or two-tailed paired *t*-tests (**c, d, f, h, i, k, m, n, p, s, v, y**), **b**: $^{**}P = 0.0034$, **c**: $^{*}P = 0.0273, 0.0374$, **i**: $^{**}P = 0.0089, 0.0056$, **o**: $^{*}P = 0.0246$, **p**: $^{*}P = 0.033, 0.0109$, **s**: $^{*}P = 0.0396$, **v**: $^{**}P = 0.0038$.

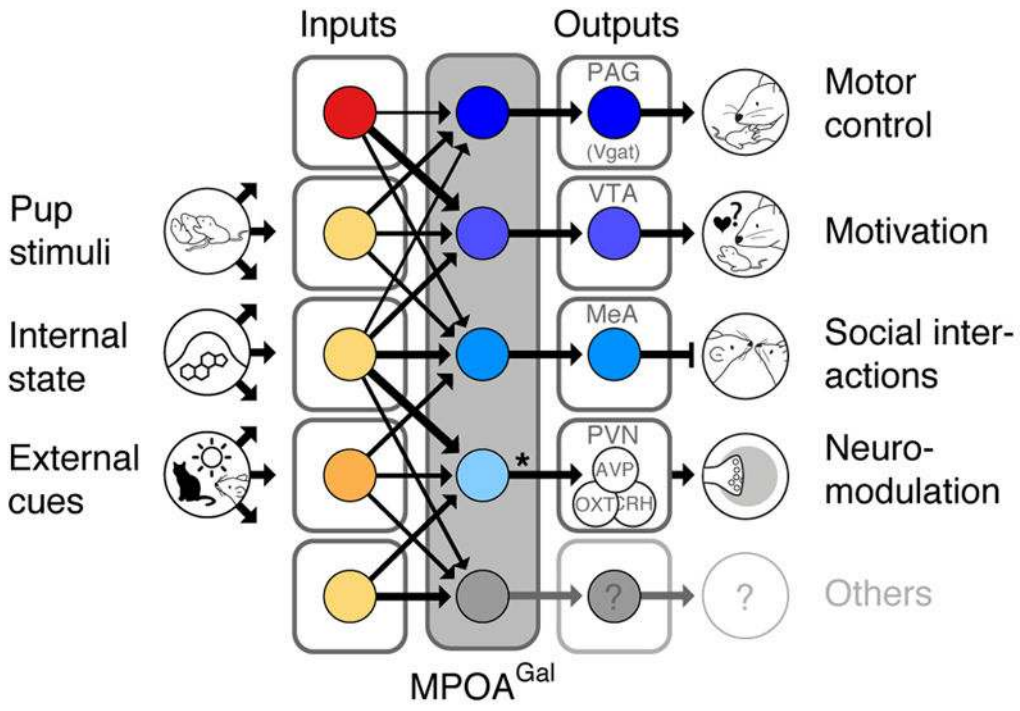

Figure 5. Functional architecture of the MPOA^{Gal} circuit

Broad, state- and sex-specifically activated inputs converge onto largely non-overlapping, projection-defined MPOA^{Gal} subpopulations that elicit specific aspects of parental behaviour. Asterisk, MPOA^{Gal}→PVN connections are sexually dimorphic (see Fig. 2e–g).